Geophys. J. Int. (2003) **152,** 318–334

Parabolic lines and caustics in homogeneous weakly anisotropic solids

Václav Vavryčuk

Geophysical Institute, Academy of Sciences of the Czech Republic, Boční II/1401, 141 31 Praha 4, *Czech Republic. E-mail: vv@ig.cas.cz*

Accepted 2002 August 2. Received 2002 August 2; in original form 2002 February 21

SUMMARY

The form of parabolic lines and caustics in homogeneous generally anisotropic solids can be very complicated, but simplifies considerably in homogeneous weakly anisotropic solids. Assuming sufficiently weak anisotropy, no parabolic lines appear on the *S*1 slowness sheet. Consequently, the corresponding wave sheet displays no caustics or triplications. Parabolic lines and caustics can appear on the *S*2 slowness and wave sheets, respectively, but only in directions close to conical or wedge singularities. Each conical and wedge singularity generates parabolic lines, caustics and anticaustics in its vicinity. The parabolic lines cannot touch or pass through a conical singularity, but they touch each wedge singularity. The size of the caustics and anticaustics decreases with decreasing strength of anisotropy. For infinitesimally weak anisotropy, the caustics and anticaustics contract into a single point. No parabolic lines, caustics, anticaustics and triplications can appear in transversely isotropic solids, provided the transverse isotropy is sufficiently weak.

Key words: anisotropy, elastic-wave theory, *P* waves, perturbation methods, ray theory, *S* waves, wave propagation.

1 INTRODUCTION

Caustics often cause difficulties in the modelling of wavefields. They produce infinite ray amplitudes, phase shifting of signals and triplications of the wave front (Kravtsov & Orlov 1990; Bakker 1998; Červený 2001). Caustics usually appear in wavefields propagating in inhomogeneous media such as gradient media or media with curved interfaces. However, in principle, they can appear even in homogeneous media, if the medium displays anisotropy (Musgrave 1970; Helbig 1994). The existence of caustics and triplications in homogeneous anisotropic media is conditioned by the existence of parabolic lines on the slowness surface. The parabolic lines (also called inflection lines) are formed by points of zero Gaussian curvature. They separate convex, concave and saddle-shaped areas on the slowness surface (Every & Kim 1994). The parabolic lines can be mapped uniquely on to caustics. Caustics (also called cusps, cuspidal lines or cuspidal edges) are formed by points of infinite Gaussian curvature on the wave surface. Hence the shape of the slowness surface fully determines the shape of the wave surface including all caustics and triplications. The form of parabolic lines and caustics in anisotropic media can be very complicated (see Figs 1 and 2) and depends on the symmetry and strength of the anisotropy. Generally, the lower the symmetry and the stronger the anisotropy, the more complicated the pattern of parabolic lines and caustics. Peculiarities in the pattern of parabolic lines and caustics also arise in the vicinity of acoustic axes (Musgrave 1985; Shuvalov & Every 1996; Boulanger & Hayes 1998; Shuvalov 1998; Wolfe 1998) also called singularity directions (Crampin & Yedlin 1981). The slowness sheets of two waves touch or intersect in these directions and can display an anomalous shape in their vicinity (Grechka & Obolentseva 1993; Vavryčuk 2001, 2002). This concerns particularly the conical singularity (Burridge 1967; Rümpker & Thomson 1994; Shuvalov & Every 1997), which is one of the most complicated singularities in anisotropy. Among the anomalies generated by the conical singularities are also 'anticaustics', defined by points of zero Gaussian curvature on the wave surface.

In this paper, we examine the form of parabolic lines and caustics in homogeneous weakly anisotropic solids. The condition of weak anisotropy is well satisfied for most rocks and geological structures in the Earth (Thomsen 1986) and considerably simplifies the problem. Obviously, if anisotropy is weak, the shape of the slowness surface should be more regular and the form of the parabolic lines and caustics should be simpler. If anisotropy vanishes and the medium becomes isotropic, the parabolic lines and caustics disappear. The shape of the slowness surface will be studied by means of the wave metric tensor (Červený 2002). This tensor can be specified under weak anisotropy using perturbation theory (Jech & Pšenčík 1989; Pšenčík 1998; Farra 2001). Perturbation theory is also used to study the metric tensor near singularities (Shuvalov 1998). The following questions are particularly addressed in this paper. Do parabolic lines and caustics disappear in weakly anisotropic solids? How do parabolic lines and caustics vary with the strength of anisotropy? Are parabolic lines and caustics connected with the existence of singularities? Can parabolic lines or caustics touch or pass through

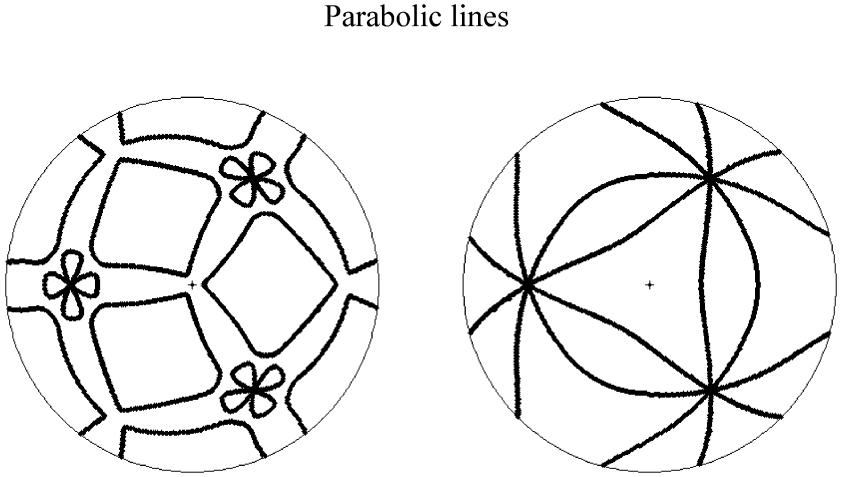

Figure 1. Parabolic lines on the slowness sheets for the $S1$ (right) and $S2$ (left) waves in strong cubic anisotropy. The parameters of anisotropy are: $a_{11} = 6.25$, $a_{44} = 2.08$, $\gamma = a_{12} - a_{11} + 2a_{44} = 2.00$. The medium is rotated so that the conical singularity is along the vertical axis. The equal-area projection is used (see Aki & Richards 1980, fig. 4.17). The cross marks the vertical axis. The bounding circles correspond to deviations of 90° of slowness directions from the vertical axis.

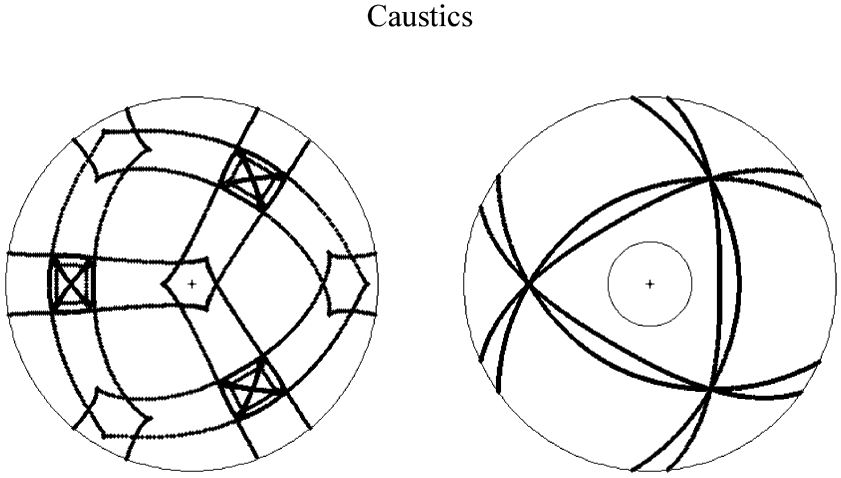

Figure 2. Caustics on the wave sheets for the $S1$ (right) and $S2$ (left) waves in strong cubic anisotropy. For parameters of the medium, see the caption of Fig. 1. The inner circle on the $S1$ sheet denotes the anticaustic. The cross marks the vertical axis. The outer circles correspond to deviations of 90° of ray directions from the vertical axis.

a singularity in weakly anisotropic solids? Can caustics touch anticaustics?

In formulae we use the following notation: lowercase Roman indices take values $i, j, \ldots = 1, 2$ and 3, and uppercase Roman indices take values $I, J, \ldots = 2$ and 3. The Einstein summation convention applies to repeated subscripts but not to repeated superscripts. Voigt two-index notation $a_{\alpha\beta}$ for density-normalized elastic parameters, with α and β running from 1 to 6, is used in parallel with the tensor notation a_{ijkl}. Several quantities are used in parallel with a bow and without a bow. The quantities accented by a bow: $\widehat{\mathbf{u}}^{(rs)}, \widehat{\mathbf{v}}^{(rs)}, \widehat{\mathbf{F}}, \widehat{\mathbf{G}}, \ldots$, are specified using an arbitrary frame of polarization vectors $\widehat{\mathbf{g}}^{0(2)}$ and $\widehat{\mathbf{g}}^{0(3)}$ of degenerate waves. The corresponding quantities without a bow: $\mathbf{u}^{(rs)}, \mathbf{v}^{(rs)}, \mathbf{F}, \mathbf{G}, \ldots$, are specified using a special frame of polarization vectors $\mathbf{g}^{0(2)}$ and $\mathbf{g}^{0(3)}$ of the degenerate waves, which satisfies continuity relations.

2 SLOWNESS AND WAVE SURFACES

The elastic properties of homogeneous anisotropic media are described by the elasticity tensor c_{ijkl} (also called the stiffness tensor) or by the density-normalized elasticity tensor $a_{ijkl} = c_{ijkl}/\rho$, where ρ is the density of the medium. These tensors control the shapes of the slowness surface S and of the wave surface W.

2.1 Slowness surface

The slowness surface S is defined by the set of all slowness vectors $\mathbf{p}(\mathbf{n}) = \mathbf{n}/c$, where $\mathbf{n}$ is the slowness direction and c is the phase velocity, which satisfy the equation (Červený 2001, eqs 2.2.35–37)

$$\det(\Gamma_{jk} - G\delta_{jk}) = 0, \tag{1}$$

where Γ_{jk} is the Christoffel tensor and G is its eigenvalue

$$G = \Gamma_{jk} g_j g_k. \tag{2}$$

The tensor Γ_{jk} is positive-definite and G is real and positive. The vector $\mathbf{g}$ is the unit polarization vector calculated as the eigenvector of Γ_{jk}. The Christoffel tensor Γ_{jk} can be defined either in terms of the slowness direction $\mathbf{n}$,

$$\Gamma_{jk}(\mathbf{n}) = a_{ijkl} n_i n_l, \tag{3}$$

or in terms of the slowness vector **p**,

$$\Gamma_{jk}(\mathbf{p}) = a_{ijkl} p_i p_l. \tag{4}$$

Eigenvalues $G(\mathbf{n})$ and $G(\mathbf{p})$ read

$$G(\mathbf{n}) = a_{ijkl} n_i n_l g_j g_k = c^2, \tag{5}$$

$$G(\mathbf{p}) = a_{ijkl} p_i p_l g_j g_k = 1. \tag{6}$$

Hereinafter, we shall implicitly assume that G and Γ_{jk} are dependent on the direction **n**, unless the dependence on slowness vector **p** is expressed explicitly.

Since the Christoffel tensor has three eigenvalues ($G^{(1)} \geq G^{(2)} \geq G^{(3)}$), the slowness surface consists of three sheets corresponding to three different waves (P, $S1$ and $S2$ waves). These sheets can be separated, but they can also touch or intersect each other. The degree of the slowness surface S is 6, thus any straight line intersects S at six points at most. This implies that any detached inner sheet of S (corresponding to the P wave) must be wholly convex, because if this were not so, a line could intersect the inner sheet at four or more points and yet make at least four further intersections with the remaining sheets (see Musgrave 1970, p. 92). In contrast to the inner sheet, the other sheets can be locally concave or saddle-shaped.

2.2 Wave surface

The wave surface W is defined by the set of all group-velocity vectors **v**, parametrized by the slowness vector $\mathbf{p}$, $\mathbf{v} = \mathbf{v}(\mathbf{p})$ or by the slowness direction $\mathbf{n}$, $\mathbf{v} = \mathbf{v}(\mathbf{n})$, which satisfy the equation (Červený 2001, eq. 2.2.65),

$$v_i = \frac{1}{2} \frac{\partial G(\mathbf{p})}{\partial p_i} = a_{ijkl} p_l g_j g_k. \tag{7}$$

The direction **N** of the group velocity, $\mathbf{N} = \mathbf{v}/\sqrt{v_i v_i}$, is called the ray direction and it differs, in general, from the slowness direction **n**.

Compared with the slowness surface S, the geometry of the wave surface W is much more complicated. The degree of W may be significantly higher than that of S (but must be less than 150; see Musgrave 1970, p. 92). If the slowness sheet of the wave in question contains saddle-shaped or concave areas, the function $\mathbf{v} = \mathbf{v}(\mathbf{N})$ can be multivalued. This means that many group-velocity vectors can correspond to one specified ray direction. This effect is known as 'triplication' of the wave surface.

2.3 Parabolic lines and caustics

It follows from eq. (7) that the geometry of the wave surface is fully controlled by the geometry of the slowness surface. The slowness surface can be convex (both principal curvatures are positive), concave (both principal curvatures are negative) or saddle-shaped (principal curvatures are of different signs). If the slowness sheet of a particular wave is wholly convex, the corresponding wave surface is also wholly convex and displays no triplications. As mentioned, triplications arise when some areas on the slowness sheets are concave or saddle-shaped. The shape of the slowness surface is conveniently indicated by the sign of the Gaussian curvature: the elliptic (convex or concave) points on a surface have a positive Gaussian curvature, the hyperbolic (saddle-shaped) points have a negative Gaussian curvature. Zero Gaussian curvature defines the parabolic points. The parabolic points form parabolic lines that are the boundaries between the convex, concave and saddle-shaped areas. Since the Gaussian curvatures of the slowness and wave surfaces are related by the following equation (Grechka & Obolentseva 1993, eq. 17; Vavryčuk & Yomogida 1996, eq. B.6)

$$K^S K^W = (\mathbf{n} \cdot \mathbf{N})^4 = \left(\frac{c}{v}\right)^4, \tag{8}$$

it is obvious that the elliptic/hyperbolic points on S are projected on to the elliptic/hyperbolic points on W (see Table 1). The parabolic points or parabolic lines with zero Gaussian curvature on S are projected on to cusps or cuspidal edges with infinite Gaussian curvature on W, called 'caustics' (see Fig. 3). Finally, points with infinite Gaussian curvature on S, which are known as conical or wedge singularities (also called conical or wedge points) are projected on to lines with zero Gaussian curvature on W, called 'anticaustics' (Shuvalov & Every 1997).

Table 1. Correspondence of shapes of the slowness and wave surfaces.

Slowness surface	Curvature K^S	Curvature K^W	Wave surface
Elliptic point (convex, concave)	$K^S > 0$	$K^W > 0$	Elliptic point (convex, concave)
Hyperbolic point (saddle-shaped)	$K^S < 0$	$K^W < 0$	Hyperbolic point (saddle-shaped)
Parabolic point	$K^S = 0$	$K^W = \pm\infty$	Caustic
Conical or wedge point	$K^S = \pm\infty$	$K^W = 0$	Anticaustic

Fig. 4 shows the geometry of the slowness and wave surfaces around a conical singularity in Payton's transverse isotropy (Payton 1992). This anisotropy forms a conical singularity along the symmetry axis. The conical singularity on the slowness surface (left-hand plots) is projected on to a circular anticaustic, which separates the wave sheets of the P and SV waves (right-hand plots). On the other hand, the circular parabolic lines separating the convex and hyperbolic areas on the slowness surface (points 1, 3, 4 and 6 in the left-hand plots) contract into conical caustics along the symmetry axis on the wave surface (right-hand plots). Note that the wave sheet for the P wave is not defined for all ray directions.

3 WAVE METRIC TENSOR IN GENERAL ANISOTROPY

The geometry of the slowness and wave surfaces can conveniently be studied using the wave metric tensor (also called the wave-propagation metric tensor), which is defined as the metric tensor in Finsler space, where the distance s is measured by the traveltime τ (Babich 1961; Hanyga 1984; Červený 2002). We define the wave metric tensor H_{il} in homogeneous anisotropic media as follows (Červený 2002, eq. 54):

$$H_{il}(\mathbf{p}) = \frac{\partial^2 H(\mathbf{p})}{\partial p_i \partial p_l} = \frac{1}{2} \frac{\partial^2 G(\mathbf{p})}{\partial p_i \partial p_l}, \tag{9}$$

where $H(\mathbf{p}) = \frac{1}{2} G(\mathbf{p})$ is the Hamiltonian and $G(\mathbf{p})$ is the eigenvalue of the Christoffel tensor $\Gamma_{jk}(\mathbf{p})$. For inhomogeneous media, the wave metric tensor $H_{il}(\mathbf{p})$, Hamiltonian $H(\mathbf{p})$ and eigenvalue $G(\mathbf{p})$ are also functions of the position vector **x**.

The determinant of the wave metric tensor H_{il} can be expressed in terms of the Gaussian curvature of the slowness surface K^S and group velocity v (Klimeš 2002, eq. 45)

$$\det(H_{il}) = v^4 K^S. \tag{10}$$

Hence, $\det(H_{il})$ is related to the shape of the slowness surface as follows: $\det(H_{il}) > 0$ corresponds to elliptic points, $\det(H_{il}) < 0$ to hyperbolic points and $\det(H_{il}) = 0$ to parabolic points on the slowness surface.

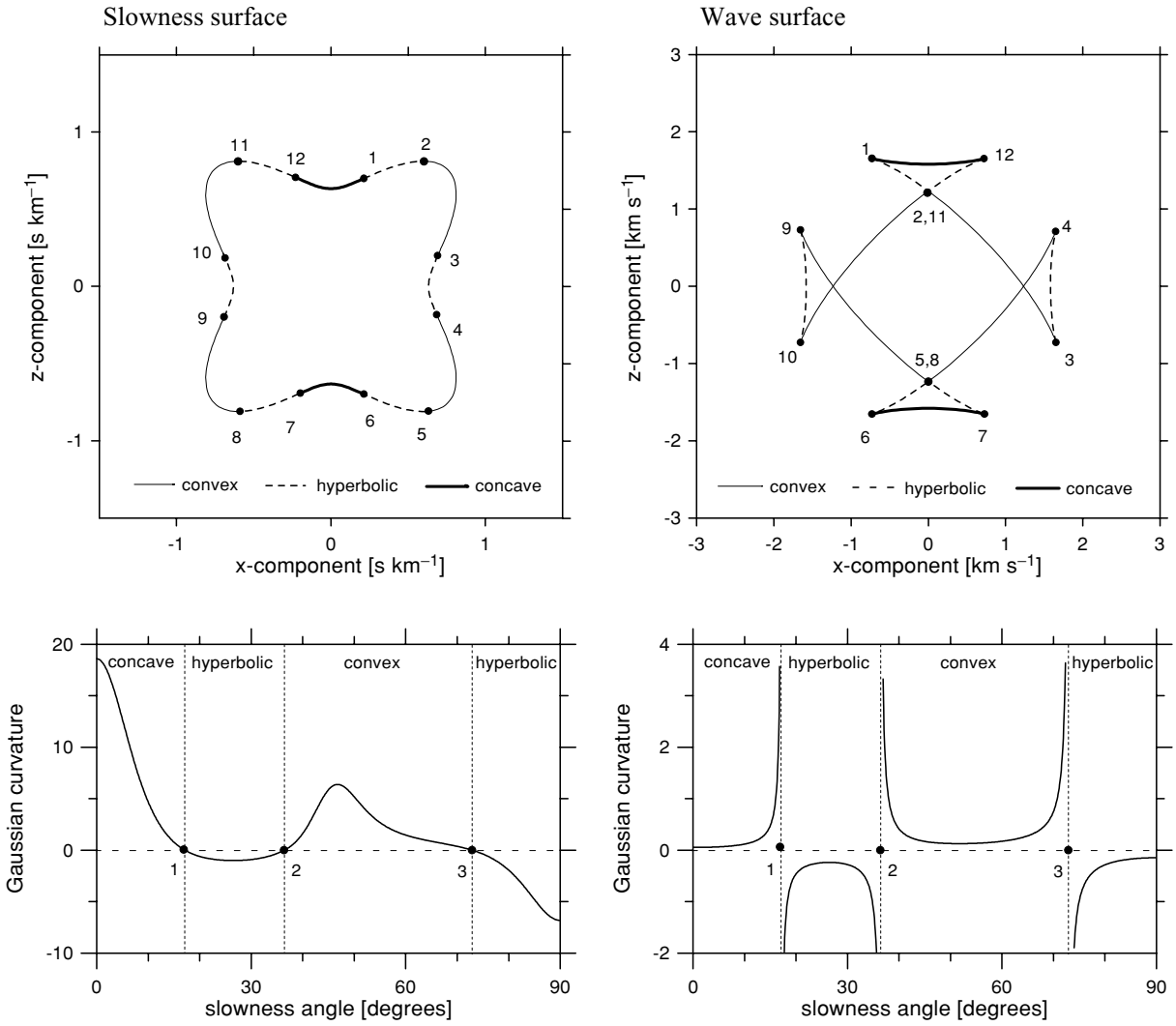

Figure 3. Parabolic points on the slowness sheet (upper left), triplications and caustics on the wave sheet (upper right) and Gaussian curvatures of the slowness (lower left) and wave (lower right) sheets for the *SV* wave in transverse isotropy. The parameters of the medium are: $a_{11} = a_{22} = a_{33} = 6.25$, $a_{44} = a_{55} = a_{66} = 2.50$, $a_{12} = 1.25$ and $a_{13} = a_{23} = 4.50$. The slowness angle is the angle between the slowness direction and the symmetry axis that coincides with the vertical axis. Parabolic points (left-hand plots) and caustics (right-hand plots) are marked by dots.

Eqs (7) and (9) can be used to express the wave metric tensor in general anisotropic media in the following form:

$$H_{il}^{(s)}(\mathbf{p}) = \frac{\partial v_i^{(s)}}{\partial p_l} = a_{ijkl} g_j^{(s)} g_k^{(s)} + a_{ijkm} p_m \frac{\partial}{\partial p_l}\left[g_j^{(s)} g_k^{(s)}\right], \tag{11}$$

where the superscript s ($s = 1, 2, 3$) denotes the type of wave (P, $S1$, $S2$). Expressing the derivative of the P-wave polarization vector $\mathbf{g}^{(1)}$ as (see Červený 2001, eqs 4.14.8–10)

$$\frac{\partial g_i^{(1)}}{\partial p_l} = \frac{\partial \Gamma_{jk}(\mathbf{p})}{\partial p_l} g_j^{(1)} \left[\frac{g_k^{(2)} g_i^{(2)}}{G^{(1)}(\mathbf{p}) - G^{(2)}(\mathbf{p})} + \frac{g_k^{(3)} g_i^{(3)}}{G^{(1)}(\mathbf{p}) - G^{(3)}(\mathbf{p})}\right], \tag{12}$$

and taking into account that

$$\frac{\partial \Gamma_{jk}(\mathbf{p})}{\partial p_l} = (a_{ijkl} + a_{ikjl}) p_i, \tag{13}$$

$$(a_{ijkl} + a_{ikjl}) p_i g_j^{(r)} g_k^{(s)} = a_{ijkl} p_i \left[g_j^{(r)} g_k^{(s)} + g_j^{(s)} g_k^{(r)}\right], \quad r, s = 1, 2, 3, \tag{14}$$

the wave metric tensor of the P wave finally reads

$$H_{il}^{(1)}(\mathbf{p}) = a_{ijkl} g_j^{(1)} g_k^{(1)} + \frac{v_i^{(12)}(\mathbf{p}) v_l^{(12)}(\mathbf{p})}{G^{(1)}(\mathbf{p}) - G^{(2)}(\mathbf{p})} + \frac{v_i^{(13)}(\mathbf{p}) v_l^{(13)}(\mathbf{p})}{G^{(1)}(\mathbf{p}) - G^{(3)}(\mathbf{p})}, \tag{15}$$

where $\mathbf{v}^{(rs)}(\mathbf{p})$, $r, s = 1, 2, 3$, is defined as

$$v_i^{(rs)}(\mathbf{p}) = a_{ijkl} p_l \left[g_j^{(r)} g_k^{(s)} + g_j^{(s)} g_k^{(r)}\right]. \tag{16}$$

For $H_{il}(\mathbf{p})$ applied to dynamic ray tracing but presented in a form slightly different from eq. (15) (see Gajewski & Pšenčík 1990).

The formulae for the metric tensors of the $S1$ and $S2$ waves are analogous to eq. (15). It can be shown that formulae (15) is invariant to substitution of $G(\mathbf{p})$ and $\mathbf{v}^{(rs)}(\mathbf{p})$ by $G(\mathbf{n})$ and $\mathbf{v}^{(rs)}(\mathbf{n})$, respectively. Hence, we express the final formulae as follows:

$$H_{il}^{(1)} = a_{ijkl} g_j^{(1)} g_k^{(1)} + \frac{v_i^{(12)} v_l^{(12)}}{G^{(1)} - G^{(2)}} + \frac{v_i^{(13)} v_l^{(13)}}{G^{(1)} - G^{(3)}}, \tag{17}$$

$$H_{il}^{(2)} = a_{ijkl} g_j^{(2)} g_k^{(2)} + \frac{v_i^{(12)} v_l^{(12)}}{G^{(2)} - G^{(1)}} + \frac{v_i^{(23)} v_l^{(23)}}{G^{(2)} - G^{(3)}}, \tag{18}$$

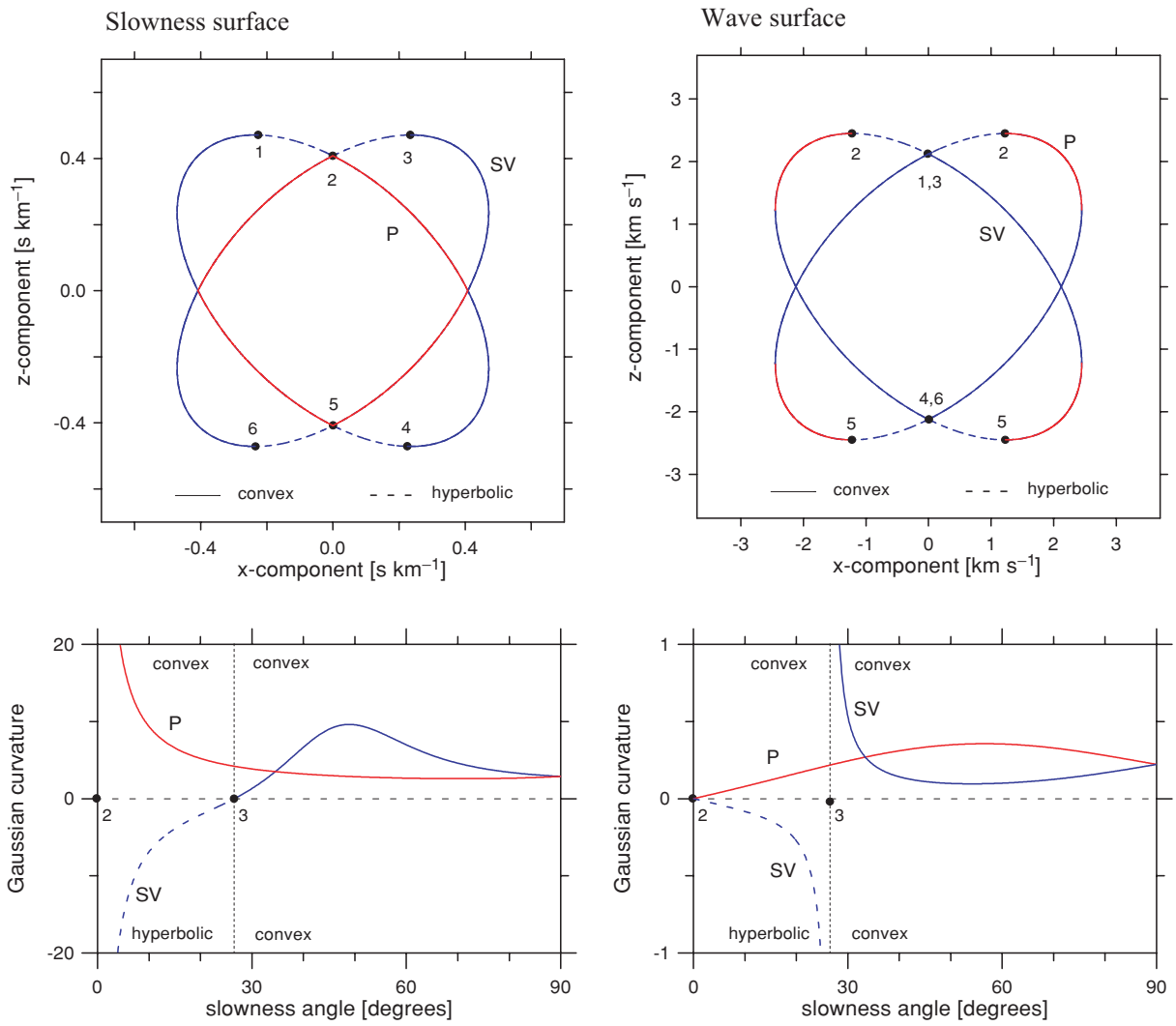

Figure 4. Vertical sections of slowness sheets (upper left) and wave sheets (upper right), and Gaussian curvatures of the slowness (lower left) and wave (lower right) sheets are shown for the *P* (red) and *SV* (blue) waves in Payton's transverse isotropy. The anisotropy displays the conical singularity along the symmetry axis. The parameters of the medium are: $a_{11} = a_{22} = a_{33} = a_{44} = a_{55} = 6.00$, $a_{66} = 3.00$ and $a_{12} = a_{13} = a_{23} = 0$. The slowness angle is the angle between the slowness direction and the symmetry axis that coincides with the vertical axis. Left-hand plots: points (1) and (3) are parabolic points, point (2) is the conical singularity. Right-hand plots: points (1) and (3) coincide with the conical caustic, point (2) marks the anticaustic.

$$H_{il}^{(3)} = a_{ijkl} g_j^{(3)} g_k^{(3)} + \frac{v_i^{(13)} v_l^{(13)}}{G^{(3)} - G^{(1)}} + \frac{v_i^{(23)} v_l^{(23)}}{G^{(3)} - G^{(2)}}, \tag{19}$$

where

$$v_i^{(rs)} = a_{ijkl} n_l \left[g_j^{(r)} g_k^{(s)} + g_j^{(s)} g_k^{(r)} \right], \tag{20}$$

$$G^{(s)} = a_{ijkl} n_i n_l g_j^{(s)} g_k^{(s)}, \tag{21}$$

and $\mathbf{g}^{(s)}$ is the polarization vector of the sth wave. Eigenvalues $G^{(1)}$, $G^{(2)}$ and $G^{(3)}$ correspond to *P*, *S*1 and *S*2 waves, respectively, satisfying the following inequality: $G^{(1)} \geq G^{(2)} \geq G^{(3)}$.

We can readily prove from eq. (17) that the *P*-wave slowness sheet must be wholly convex. Taking into account that: (1) the tensor $a_{ijkl} g_j^{(1)} g_k^{(1)}$ is positive-definite (which follows from the positive-definiteness of Γ_{il}), (2) the dyad $v_i^{(rs)} v_l^{(rs)}$ has two zero eigenvalues and one non-zero eigenvalue that is always positive and (3) eigenvalue $G^{(1)}$ is greater than or equal to $G^{(2)}$ and $G^{(3)}$, we find that $\det(H_{il}^{(1)})$ must be positive for any slowness direction $\mathbf{n}$. Hence, we can generalize the result obtained by (Musgrave 1970, p. 92) regarding the convexity of the *P*-wave slowness sheet: *the P-wave slowness sheet must be convex even in cases where it touches the slowness sheets of one or two S waves*.

However, no conclusion similar to that for the *P* wave can be drawn for the *S*1 or *S*2 waves. As regards the *S*1 wave, the second term in eq. (18) has a negative denominator and can cause $\det(H_{il}^{(2)})$ to be zero or negative for some slowness directions $\mathbf{n}$. As regards the *S*2 wave, both the second and third terms in eq. (19) have negative denominators and can cause $\det(H_{il}^{(3)})$ to be zero or negative for some slowness directions $\mathbf{n}$. Therefore, parabolic lines can appear on the *S*1- and the *S*2-wave slowness sheets. Furthermore, we can expect the concave or hyperbolic areas on the slowness sheets to be larger for the *S*2 wave than for the *S*1 wave, and the parabolic lines to be, in general, more complicated for the *S*2 wave than for the *S*1 wave. Subsequently, the geometry of the wave sheet for the *S*2 wave should also be more complicated than that for the *S*1 wave.

Compared with anisotropy, the wave metric tensor H_{il} is much simpler under isotropy. Taking into account that the group velocity reads

$$v_i = c^2 p_i, \tag{22}$$

we obtain

$$H_{il}^{\rm iso} = \frac{\partial v_i}{\partial p_l} = c^2 \delta_{il}, \tag{23}$$

where c is the phase velocity of the wave and δ_{il} is the Kronecker delta. Hence det $(H_{il}^{\rm iso})$ is always positive. Obviously, the slowness sheets are wholly convex and no parabolic lines can appear for P or S waves in homogeneous isotropic media.

4 PARABOLIC LINES IN WEAK ANISOTROPY

Here, we study the determinant of the metric tensor H_{il} for the $S1$ and $S2$ waves in weakly anisotropic media. By 'weak anisotropy' we mean that the elastic parameters of the medium can be expressed in the following form:

$$a_{ijkl} = a^0_{ijkl} + \Delta a_{ijkl}, \tag{24}$$

$$a^0_{ijkl} = (\alpha^2 - 2\beta^2)\delta_{ij}\delta_{kl} + \beta^2(\delta_{ik}\delta_{jl} + \delta_{il}\delta_{jk}), \tag{25}$$

where α and β are the P- and S-wave velocities in an isotropic reference medium, δ_{ij} is the Kronecker delta, and Δa_{ijkl} are small perturbations ($\Delta a_{ijkl} \to 0$) from the parameters of the isotropic reference medium a^0_{ijkl}.

Since det(H_{il}) is very simple under isotropy, eq. (23), we might reasonably anticipate that it will not be very complicated even under weak anisotropy. To prove this we apply first-order perturbation theory. Since the Christoffel tensor Γ_{jk} is degenerate for S waves under isotropy, we apply the perturbation theory for a degenerate Christoffel eigenvalue problem (see Appendix A) and specify the eigenvalues and eigenvectors of Γ_{jk} under weak anisotropy (see Appendix B). We can then linearize all of the necessary quantities in eqs (18) and (19) to derive the metric tensors for the $S1$ and $S2$ waves.

Linearizing the $S1$-wave metric tensor $H^{(2)}_{il}$ given in eq. (18) for weakly anisotropic media, eq. (24), we obtain (see Appendix D)

$$H^{(2)}_{il} = H^{0(2)}_{il} + \Delta H^{(2)}_{il}, \tag{26}$$

where $H^{0(2)}_{il}$ denotes the leading term of the wave metric tensor and $\Delta H^{(2)}_{il}$ denotes its perturbation,

$$H^{0(2)}_{il} = \beta^2 \delta_{il}, \tag{27}$$

$$\begin{aligned}\Delta H^{(2)}_{il} = {} & \Delta a_{ijkl} g^{0(2)}_j g^{0(2)}_k + (\alpha^2 - \beta^2)\left[\Delta g^{(2)}_i g^{0(2)}_l + g^{0(2)}_i \Delta g^{(2)}_l\right] \\ & - g^{0(2)}_i \Delta v^{(12)}_l - g^{0(2)}_l \Delta v^{(12)}_i - g^{0(2)}_i g^{0(2)}_l \left[\Delta G^{(2)} - \Delta G^{(1)}\right] \\ & + \frac{\Delta v^{(23)}_i \Delta v^{(23)}_l}{\Delta G}.\end{aligned} \tag{28}$$

The perturbations $\Delta \mathbf{g}^{(s)}$, ΔG and $\Delta G^{(s)}$, $s = 1, 2, 3$ are defined in Appendix B, and the perturbation $\Delta \mathbf{v}^{(rs)}$ is defined in eq. (D16). Vectors $\mathbf{g}^{0(s)}$, $s = 1, 2, 3$ are polarization vectors in the isotropic reference medium: vector $\mathbf{g}^{0(1)}$ is the P-wave polarization vector coinciding with vector $\mathbf{n}$, and vectors $\mathbf{g}^{0(2)}$ and $\mathbf{g}^{0(3)}$ form a special frame of orthonormal vectors perpendicular to $\mathbf{g}^{0(1)}$ satisfying the following continuity relations (see Appendix B):

$$\mathbf{g}^{(J)}(a_{ijkl}, n_i) \to \mathbf{g}^{0(J)}\left(a^0_{ijkl}, n_i\right), \quad J = 2, 3, \tag{29}$$

for vanishing anisotropy, $a_{ijkl} \to a^0_{ijkl}$, and for fixed slowness direction $\mathbf{n}$.

The formulae for the components of the linearized $S2$-wave metric tensor $H^{0(3)}_{il}$ are analogous to eqs (26–28). Finally, we arrive at the expression for det$(H^{(J)}_{il})$, $J = 2, 3$:

$$\begin{aligned}\det\left(H^{(J)}_{il}\right) &= \begin{vmatrix} \beta^2 + \Delta H^{(J)}_{11} & \Delta H^{(J)}_{12} & \Delta H^{(J)}_{13} \\ \Delta H^{(J)}_{12} & \beta^2 + \Delta H^{(J)}_{22} & \Delta H^{(J)}_{23} \\ \Delta H^{(J)}_{13} & \Delta H^{(J)}_{23} & \beta^2 + \Delta H^{(J)}_{33} \end{vmatrix} \\ &\cong \beta^6 \left[1 + \frac{\Delta H^{(J)}_{ii}}{\beta^2}\right],\end{aligned} \tag{30}$$

$$\begin{aligned}\Delta H^{(2)}_{ii} = {} & \Delta a_{ijki} g^{0(2)}_j g^{0(2)}_k - 2 g^{0(2)}_i \Delta v^{(12)}_i - \Delta G^{(2)} \\ & + \Delta G^{(1)} + \frac{\Delta v^{(23)}_i \Delta v^{(23)}_i}{\Delta G},\end{aligned} \tag{31}$$

$$\begin{aligned}\Delta H^{(3)}_{ii} = {} & \Delta a_{ijki} g^{0(3)}_j g^{0(3)}_k - 2 g^{0(3)}_i \Delta v^{(13)}_i - \Delta G^{(3)} \\ & + \Delta G^{(1)} - \frac{\Delta v^{(23)}_i \Delta v^{(23)}_i}{\Delta G},\end{aligned} \tag{32}$$

where we have omitted all terms with second- or higher-order perturbations and used the following identity:

$$g^{0(J)}_i \Delta g^{(J)}_i = 0, \quad J = 2, 3. \tag{33}$$

The perturbation $\Delta \mathbf{v}^{(rs)}$ is defined in eq. (D16), and the perturbations ΔG, $\Delta G^{(s)}$ and $\Delta \mathbf{g}^{(s)}$ in Appendix B.

Assume that the slowness direction $\mathbf{n}$ is not in the vicinity of an S-wave singularity. Hence the slowness sheets of the $S1$ and $S2$ waves are non-degenerate ($\Delta G \neq 0$) and they do not touch or intersect each other in the vicinity of $\mathbf{n}$. Then all terms on the right-hand sides of eqs (31) and (32) are small because they are linear functions of small quantities Δa_{ijkl}. Hence

$$\frac{\Delta H^{(J)}_{ii}}{\beta^2} \ll 1, \quad J = 2, 3. \tag{34}$$

This implies that det$(H^{(J)}_{il})$ in eq. (30) must be positive and the slowness sheets of the $S1$ or $S2$ waves must be convex in the directions studied. In other words, no parabolic lines can appear on the $S1$ or $S2$ slowness sheets in weakly anisotropic media except for directions close to S-wave singularities. In the singularities ($\Delta G = 0$) and in their vicinities, the final term in eqs (31) and (32) may be large or even infinite. Since the sign of this term is positive for the $S1$ wave, det$(H^{(2)}_{il})$ must also be positive in directions near singularities. Consequently, no parabolic lines can appear on the $S1$-wave slowness surface in weakly anisotropic media regardless of direction or the presence of singularities. On the other hand, the sign of the final term in eq. (32) is negative for the $S2$ wave and this may cause det$(H^{(3)}_{il})$ to be zero or negative in the vicinity of a singularity. Therefore, in this case the behaviour of $H^{(3)}_{il}$ requires special analysis.

5 PARABOLIC LINES NEAR SINGULARITIES IN WEAK ANISOTROPY

Examination of the shape of the $S2$-wave slowness sheet in weakly anisotropic media near S-wave singularities requires special treatment. In regular directions, small perturbations Δa_{ijkl} result in small perturbations of all basic quantities of the wavefields, including the shapes of the slowness and wave surfaces. In directions close to a singularity, the behaviour of the polarization vectors is anomalous and can also cause anomalies in the shapes of the slowness and wave surfaces. As regards the wave metric tensor $H^{(3)}_{il}$, defined in eq. (19), the anomalies are caused by the following term:

$$H_{il}^{(23)} = \frac{v_i^{(23)} v_l^{(23)}}{\Delta G}, \tag{35}$$

because its denominator $\Delta G = G^{(2)} - G^{(3)}$ is zero at the singularity. The anomalous behaviour of $H_{il}^{(23)}$ near singularities can be studied using perturbation theory, but in a slightly modified way compared with the previous section. So far, we have fixed the slowness direction $\mathbf{n}$ and perturbed the elastic parameters a_{ijkl},

$$a_{ijkl} = a_{ijkl}^0 + \Delta a_{ijkl}, \tag{36}$$

to obtain the quantities in weak anisotropy expressed in terms of those in the isotropic reference medium (see Fig. 5a). Now, we fix the elastic parameters a_{ijkl} of an anisotropic medium and perturb the slowness direction $\mathbf{n}$

$$\mathbf{n} = \mathbf{n}^0 + \Delta \mathbf{n}, \tag{37}$$

to obtain the quantities in the close vicinity of the singularity expressed in terms of those at the singularity (see Fig. 5b). The approaches are very similar, because the Christoffel tensor Γ_{jk} is degenerate in isotropy and at the singularity. Therefore, perturbation theory for a degenerate Christoffel eigenvalue problem (see Appendix A) has to be applied in both cases. However, the specification

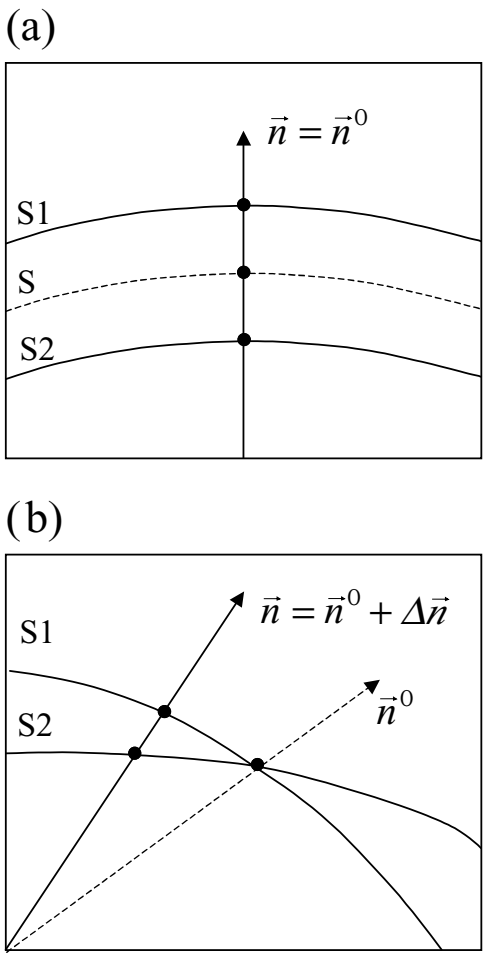

Figure 5. First-order perturbation theory applied to weak anisotropy (a) and to near-singularity directions (b). Quantities on the *S*1 and *S*2 slowness sheets in (a) are calculated by perturbing quantities on the isotropic *S* slowness sheet (dashed line). Quantities on the *S*1 and *S*2 slowness sheets in (b) are calculated by perturbing quantities at the singularity direction $\mathbf{n}^0$ (dashed line).

of the general formulae for eigenvalues and eigenvectors of Γ_{jk} is different for eqs (36) and (37). The perturbation formulae obtained using eq. (36) are given in Appendix B and those obtained using eq. (37) are given in Appendix C. Using the formulae in Appendix C we can perturb $H_{il}^{(23)}$ in eq. (35) to inspect its properties in the vicinity of a singularity. Perturbing $H_{il}^{(23)}$ we obtain

$$H_{il}^{(23)} = H_{il}^{0(23)} + \Delta H_{il}^{(23)}, \tag{38}$$

where $H_{il}^{0(23)}$ denotes the value of $H_{il}^{(23)}$ at the singularity and $\Delta H_{il}^{(23)}$ is its perturbation. Taking into account eq. (35) we obtain

$$H_{il}^{0(23)} = \lim_{\Delta G \to 0} \frac{v_i^{0(23)} v_l^{0(23)}}{\Delta G}, \tag{39}$$

$$\Delta H_{il}^{(23)} = \frac{v_i^{0(23)} \Delta v_l^{(23)} + \Delta v_i^{(23)} v_l^{0(23)} + \Delta v_i^{(23)} \Delta v_l^{(23)}}{\Delta G}, \tag{40}$$

where

$$\begin{aligned} v_i^{0(23)} &= a_{ijkl} n_l^0 \left[g_j^{0(2)} g_k^{0(3)} + g_j^{0(3)} g_k^{0(2)} \right], \\ \Delta v_i^{(23)} &= a_{ijkl} \Delta n_l \left[g_j^{0(2)} g_k^{0(3)} + g_j^{0(3)} g_k^{0(2)} \right] + a_{ijkl} n_l^0 \left[\Delta g_j^{(2)} g_k^{0(3)} \right. \\ &\quad \left. + g_j^{0(2)} \Delta g_k^{(3)} + \Delta g_j^{(3)} g_k^{0(2)} + g_j^{0(3)} \Delta g_k^{(2)} \right]. \end{aligned} \tag{41}$$

The vectors $\mathbf{g}^{0(2)}$ and $\mathbf{g}^{0(3)}$ form a special frame of orthonormal vectors perpendicular to $\mathbf{g}^{0(1)}$ satisfying the following continuity relations:

$$\mathbf{g}^{(J)}(a_{ijkl}, n_i) \to \mathbf{g}^{0(J)}(a_{ijkl}, e_l), \quad J = 2, 3, \tag{42}$$

for $\mathbf{n}$ approaching the singularity direction $\mathbf{n}^0$. Vector $\mathbf{e}$ is the unit vector that is perpendicular to the singularity direction $\mathbf{n}^0$ and which specifies the direction of approach to the singularity. Note that $\mathbf{v}^{0(23)}$ and $\Delta\mathbf{v}^{(23)}$ defined in eq. (41) are slightly different quantities from those used in Section 4.

Below, we evaluate $H_{il}^{0(23)}$ and $\Delta H_{il}^{(23)}$ for four kinds of *S*-wave singularity: kiss, conical, wedge and intersection singularities.

5.1 Kiss singularity

The kiss singularity is defined as the direction in which the slowness sheets of two waves touch tangentially at an isolated point. The wave sheets are also tangential at the kiss singularity and the group velocities coincide for both waves. The condition for this singularity can be expressed as follows (Shuvalov 1998):

$$\widehat{\mathbf{u}}^{0(23)} = 0, \quad \widehat{\mathbf{v}}^{0(23)} = 0, \tag{43}$$

where $\widehat{\mathbf{u}}^{0(23)}$ and $\widehat{\mathbf{v}}^{0(23)}$ are given by

$$\begin{aligned} \widehat{u}_i^{0(23)} &= a_{ijkl} n_l^0 \left[\widehat{g}_j^{0(2)} \widehat{g}_k^{0(2)} - \widehat{g}_j^{0(3)} \widehat{g}_k^{0(3)} \right], \\ \widehat{v}_i^{0(23)} &= a_{ijkl} n_l^0 \left[\widehat{g}_j^{0(2)} \widehat{g}_k^{0(3)} + \widehat{g}_j^{0(3)} \widehat{g}_k^{0(2)} \right]. \end{aligned} \tag{44}$$

The vector $\mathbf{n}^0$ specifies the singularity direction, and vectors $\widehat{\mathbf{g}}^{0(2)}$ and $\widehat{\mathbf{g}}^{0(3)}$ form an arbitrary frame of orthogonal unit vectors perpendicular to the *P*-wave polarization vector at the singularity. From eqs (C4) and (C8) we obtain for the leading terms ΔG and Φ:

$$\Delta G = \vartheta^2 \sqrt{(\mathbf{e}^{\mathrm{T}} \widehat{\mathbf{F}} \mathbf{e})^2 + (\mathbf{e}^{\mathrm{T}} \widehat{\mathbf{G}} \mathbf{e})^2}, \quad \vartheta \ll 1, \tag{45}$$

$$\tan 2\Phi = \frac{\mathbf{e}^{\mathrm{T}}\widehat{\mathbf{G}}\mathbf{e}}{\mathbf{e}^{\mathrm{T}}\widehat{\mathbf{F}}\mathbf{e}}, \tag{46}$$

where $\mathbf{e}$ is the unit vector specifying the direction from which the singularity is approached. The angle ϑ is the angle between the slowness direction $\mathbf{n}$ and the singularity direction $\mathbf{n}^0$ (see Fig. 6). Matrices $\widehat{\mathbf{F}}$ and $\widehat{\mathbf{G}}$ are defined in eqs (C6) and (C7). Since $\widehat{\mathbf{v}}^{0(23)}$ in eq. (43) is zero for any frame of vectors $\widehat{\mathbf{g}}^{0(2)}$ and $\widehat{\mathbf{g}}^{0(3)}$, it must be zero also for the base vectors $\mathbf{g}^{0(2)}$ and $\mathbf{g}^{0(3)}$:

$$\mathbf{v}^{0(23)} = 0. \tag{47}$$

Inserting eq. (47) into eqs (38–40) we obtain for the leading term of $H_{il}^{(23)}$,

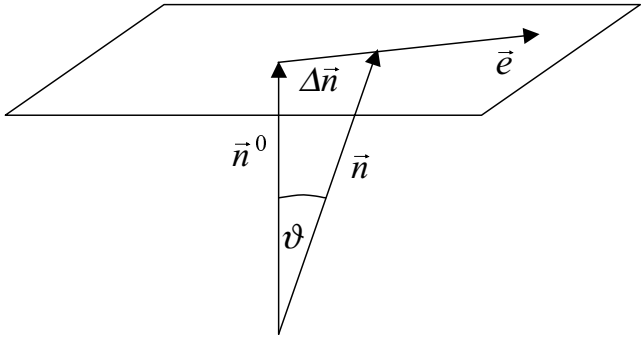

Figure 6. Definition of vectors near the singularity direction $\mathbf{n}^0$.

$$H_{il}^{(23)} = \frac{\Delta v_i^{(23)} \Delta v_l^{(23)}}{\Delta G}. \tag{48}$$

Since $\Delta\mathbf{v}^{(23)}$ defined in eq. (41) is a first-order quantity in ϑ, and ΔG in eq. (45) is a second-order quantity in ϑ, the leading term of $H_{il}^{(23)}$ is independent of ϑ. Hence, $H_{il}^{(23)}$ is finite in the kiss singularity and in its close vicinity, but it is not necessarily small. Therefore, this term can generate parabolic lines crossing the kiss singularity on the $S2$-wave slowness sheet. However, this concerns the strong anisotropy only, because if we assume weak anisotropy and apply a similar approach as in Section 4, we can prove that $\Delta\mathbf{v}^{(23)}$ and ΔG are also first-order perturbations in Δa_{ijkl}. Consequently, $H_{il}^{(23)}$ must be small,

$$H_{il}^{(23)} = \frac{\Delta v_i^{(23)} \Delta v_l^{(23)}}{\Delta G} \ll 1. \tag{49}$$

Hence, under weak anisotropy no parabolic lines can appear on the $S2$-wave slowness sheet in the kiss singularity or in its vicinity.

5.2 Conical singularity

The conical singularity is defined as the isolated direction in which two slowness sheets touch through the vertices of cone-shaped surfaces. The condition for this singularity can be expressed by means of the vector product of $\widehat{\mathbf{u}}^{0(23)}$ and $\widehat{\mathbf{v}}^{0(23)}$ as follows (Shuvalov 1998):

$$\widehat{\mathbf{u}}^{0(23)} \times \widehat{\mathbf{v}}^{0(23)} \neq 0, \tag{50}$$

where $\widehat{\mathbf{u}}^{0(23)}$ and $\widehat{\mathbf{v}}^{0(23)}$ are defined in eq. (44). From eqs (C4) and (C8) we obtain for the leading terms of ΔG and Φ

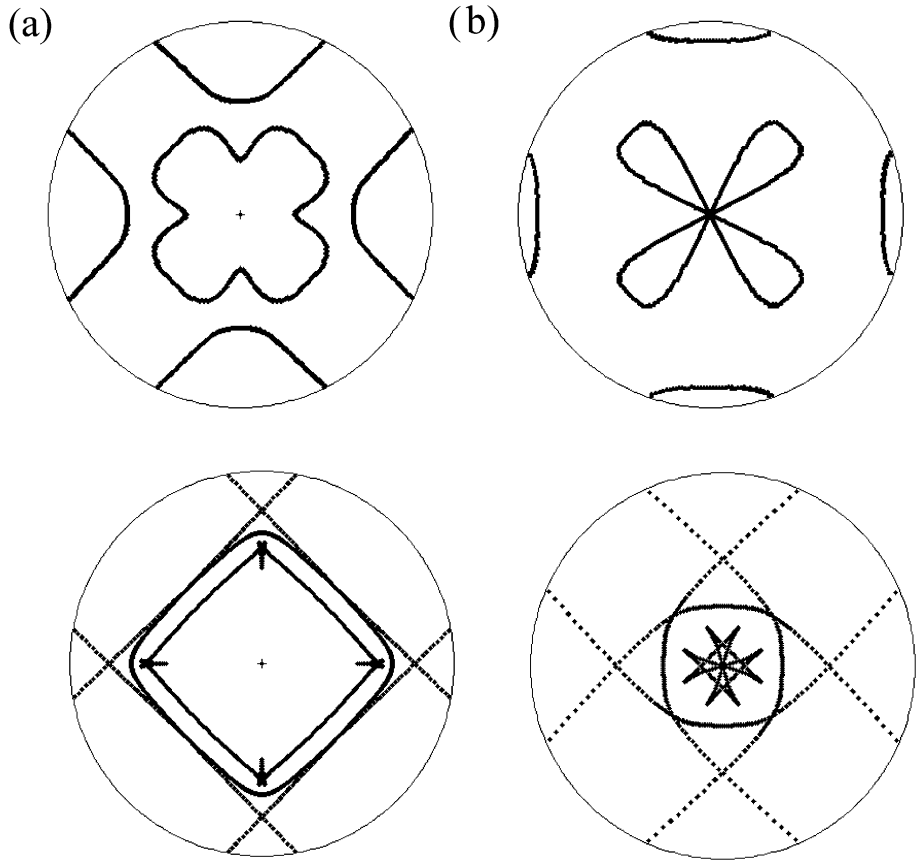

Figure 7. Parabolic lines (upper plots) and caustics (lower plots) for the $S2$ wave near the kiss singularity in cubic anisotropy. Parameters of anisotropy are: $a_{11} = 6.25$, $a_{44} = 2.08$, (a) $\gamma = 2.50$, (b) $\gamma = 1.38$. The cross denotes the kiss singularity that coincides with the vertical axis. The bounding circles correspond to the deviation (a) $\theta = 30^\circ$, (b) $\theta = 13^\circ$ of the slowness directions (upper plots) or ray directions (lower plots) from the vertical axis.

$$\Delta G = 2\vartheta\sqrt{(\widehat{\mathbf{u}}^{0(23)}\cdot\mathbf{e})^2+\left(\widehat{\mathbf{v}}^{0(23)}\cdot\mathbf{e}\right)^2}, \tag{51}$$

$$\tan 2\Phi = \frac{\widehat{\mathbf{v}}^{0(23)}\cdot\mathbf{e}}{\widehat{\mathbf{u}}^{0(23)}\cdot\mathbf{e}}. \tag{52}$$

The vector **e** is the unit vector specifying the direction from which the singularity is approached. The angle ϑ is the angle between the slowness direction **n** and the singularity direction $\mathbf{n}^0$ (see Fig. 6). It follows from eq. (50) that $\widehat{\mathbf{v}}^{0(23)}$ is non-zero. This applies to any frame of vectors $\widehat{\mathbf{g}}^{0(2)}$ and $\widehat{\mathbf{g}}^{0(3)}$, including vectors $\mathbf{g}^{0(2)}$ and $\mathbf{g}^{0(3)}$, hence

$$\mathbf{v}^{0(23)} \neq 0. \tag{53}$$

Since ΔG goes to zero at the singularity ($\vartheta \to 0$), we obtain from eq. (39)

$$H_{il}^{0(23)} = \lim_{\Delta G\to 0}\frac{v_i^{0(23)}v_l^{0(23)}}{\Delta G} = \infty. \tag{54}$$

This implies that, in approaching the singularity,

$$\det\left(H_{il}^{(2)}\right) \to \infty, \tag{55}$$

$$\det\left(H_{il}^{(3)}\right) \to -\infty. \tag{56}$$

Since $\det(H_{il}^{(3)})$ is minus infinity at the singularity, but is positive outside the vicinity of the singularity, there must exist directions near the singularity for which $\det(H_{il}^{(3)})$ is zero. This implies that the parabolic line forms a closed curve around the singularity. The shape and size of the parabolic line depends on the symmetry and strength of the anisotropy. As the strength of the anisotropy decreases, the parabolic line should contract, becoming increasingly close to the singularity. Under infinitely weak anisotropy, the parabolic line and the singularity merge and disappear.

5.3 Wedge singularity

The wedge singularity is defined as the isolated direction in which two slowness sheets touch through the vertices of wedge-shaped surfaces. The wedge singularity can arise from the conical singularity if one of the semi-axes of the elliptical base of the cone goes to infinity. The condition for this singularity can be expressed as follows (Shuvalov 1998):

$$\widehat{\mathbf{u}}^{0(23)}\times\widehat{\mathbf{v}}^{0(23)} = 0, \qquad \widehat{\mathbf{u}}^{0(23)}\cdot\widehat{\mathbf{u}}^{0(23)} + \widehat{\mathbf{v}}^{0(23)}\cdot\widehat{\mathbf{v}}^{0(23)} \neq 0, \tag{57}$$

where $\widehat{\mathbf{u}}^{0(23)}$ and $\widehat{\mathbf{v}}^{0(23)}$ are parallel vectors perpendicular to the direction **t** of the wedge

$$\widehat{\mathbf{u}}^{0(23)} || \widehat{\mathbf{v}}^{0(23)} \perp \mathbf{t}. \tag{58}$$

Hence the direction of the vectors $\widehat{\mathbf{u}}^{0(23)}$ and $\widehat{\mathbf{v}}^{0(23)}$ is independent of the base vectors $\widehat{\mathbf{g}}^{0(2)}$ and $\widehat{\mathbf{g}}^{0(3)}$ used in eq. (44).

The wedge singularity combines the properties of the kiss and conical singularities. For direction **e** along **t,**

$$\widehat{\mathbf{u}}^{0(23)}\cdot\mathbf{e} = 0, \quad \widehat{\mathbf{v}}^{0(23)}\cdot\mathbf{e} = 0, \tag{59}$$

for any frame of vectors $\widehat{\mathbf{g}}^{0(2)}$ and $\widehat{\mathbf{g}}^{0(3)}$ used in eq. (44). Hence, the leading terms of ΔG and Φ are expressed by eqs (45) and (46)

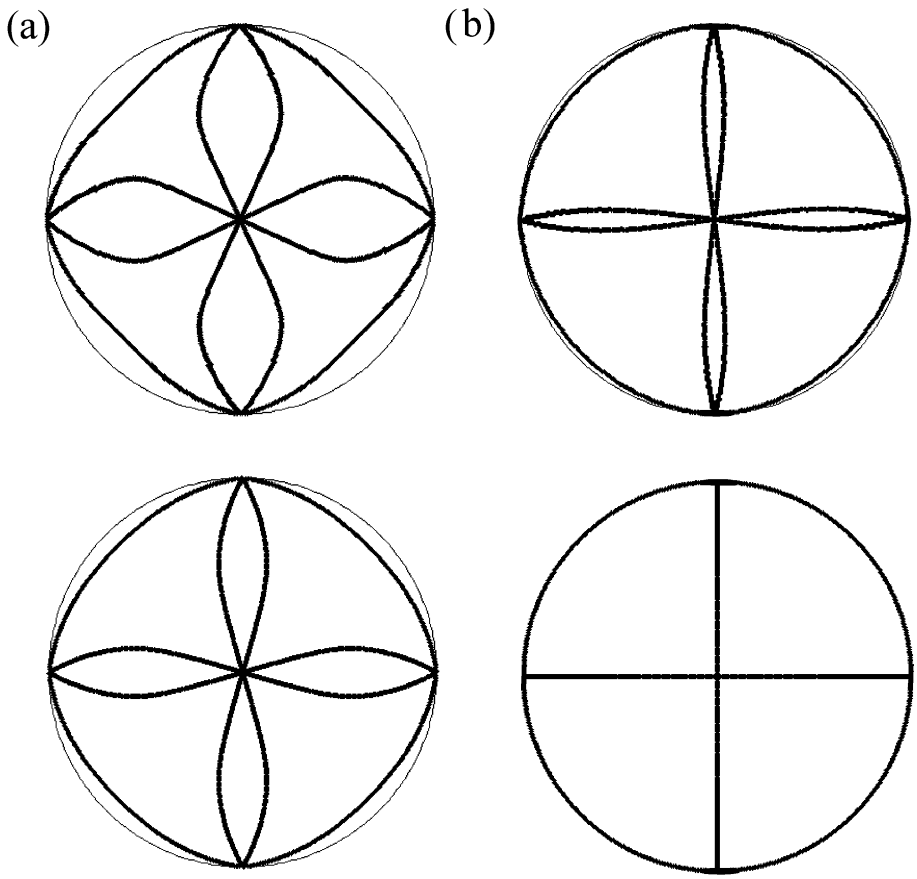

Figure 8. Parabolic lines (upper plots) and caustics (lower plots) for the *S*1 wave near the kiss singularity in cubic anisotropy. The parameters of anisotropy are: $a_{11} = 6.25$, $a_{44} = 2.08$, (a) $\gamma = 2.50$, (b) $\gamma = 1.38$. The kiss singularity coincides with the vertical axis. The bounding circles correspond to the deviation $\theta = 90^\circ$ of the slowness directions (upper plots) or ray directions (lower plots) from the vertical axis.

derived for the kiss singularity. For direction **e** perpendicular to **t**, we can always find a frame of vectors $\widehat{\mathbf{g}}^{0(2)}$ and $\widehat{\mathbf{g}}^{0(3)}$, for which

$$\widehat{\mathbf{u}}^{0(23)} \cdot \mathbf{e} \neq 0, \quad \widehat{\mathbf{v}}^{0(23)} \cdot \mathbf{e} \neq 0. \tag{60}$$

Hence the leading terms of ΔG and Φ are expressed by eqs (51) and (52) derived for the conical singularity. It can be shown that $\mathbf{v}^{0(23)}$ in eqs (39) and (40) is zero for $\mathbf{e} \perp \mathbf{t}$, but non-zero for $\mathbf{e} \parallel \mathbf{t}$. Therefore, assuming weak anisotropy and approaching the singularity we obtain for $\mathbf{e} \perp \mathbf{t}$,

$$H_{il}^{(23)} \to 0, \quad \det\left(H_{il}^{(3)}\right) \to \beta^6, \tag{61}$$

and for $\mathbf{e} \parallel \mathbf{t}$,

$$H_{il}^{0(23)} \to \infty, \quad \det\left(H_{il}^{(3)}\right) \to -\infty. \tag{62}$$

Hence, the $S2$-wave slowness sheet is always convex for directions **e** perpendicular to the wedge direction **t**, but saddle-shaped for **e** parallel to **t**. This implies that the wedge singularity generates parabolic lines in weakly anisotropic solids. These lines must always touch the singularity.

5.4 Intersection singularity

The intersection singularity occurs when the slowness sheets of the $S1$ and $S2$ waves intersect along a line. This singularity is, in fact, a line wedge singularity. The condition for this singularity can be expressed as follows (Shuvalov 1998, eq. 2.61):

$$\widehat{\mathbf{v}}^{0(23)} = \eta \widehat{\mathbf{u}}^{0(23)}, \quad \mathbf{e}^{\mathrm{T}} \widehat{\mathbf{G}} \mathbf{e} = \eta \mathbf{e}^{\mathrm{T}} \widehat{\mathbf{F}} \mathbf{e}, \tag{63}$$

where η is a constant, vectors $\widehat{\mathbf{u}}^{0(23)}$ and $\widehat{\mathbf{v}}^{0(23)}$ are defined in eq. (44), and the matrices $\widehat{\mathbf{F}}$ and $\widehat{\mathbf{G}}$ are defined in eqs (C6) and (C7). The base vectors $\widehat{\mathbf{g}}^{0(2)}$ and $\widehat{\mathbf{g}}^{0(3)}$ in eq. (63) must be chosen to yield

$$\left|\widehat{\mathbf{u}}^{0(23)}\right| \neq 0. \tag{64}$$

Using eqs (C4) and (C8), we can express the leading terms of ΔG and Φ as follows:

$$\Delta G = 2\vartheta \left(\widehat{\mathbf{u}}^{0(23)} \cdot \mathbf{e}\right) \sqrt{1+\eta^2}, \tag{65}$$

$$\tan 2\Phi = \eta. \tag{66}$$

The intersection singularity displays no singular behaviour of the polarization vectors in its vicinity (Shuvalov 1998), hence the angle Φ is constant and does not depend on the direction **e** from which the singularity is approached. The angle Φ only depends on the choice of base vectors $\widehat{\mathbf{g}}^{0(2)}$ and $\widehat{\mathbf{g}}^{0(3)}$ at the singularity. If we use base vectors $\mathbf{g}^{0(2)}$ and $\mathbf{g}^{0(3)}$ at the singularity, the angle Φ is zero (see eq. C13). Subsequently, η in eq. (66) is also zero, and eq. (63) yields

$$\mathbf{v}^{0(23)} = 0 \tag{67}$$

for any vector **e**. Inserting eq. (67) into eqs (38–40) we obtain

$$H_{il}^{(23)} = \frac{\Delta v_i^{(23)} \Delta v_l^{(23)}}{\Delta G}. \tag{68}$$

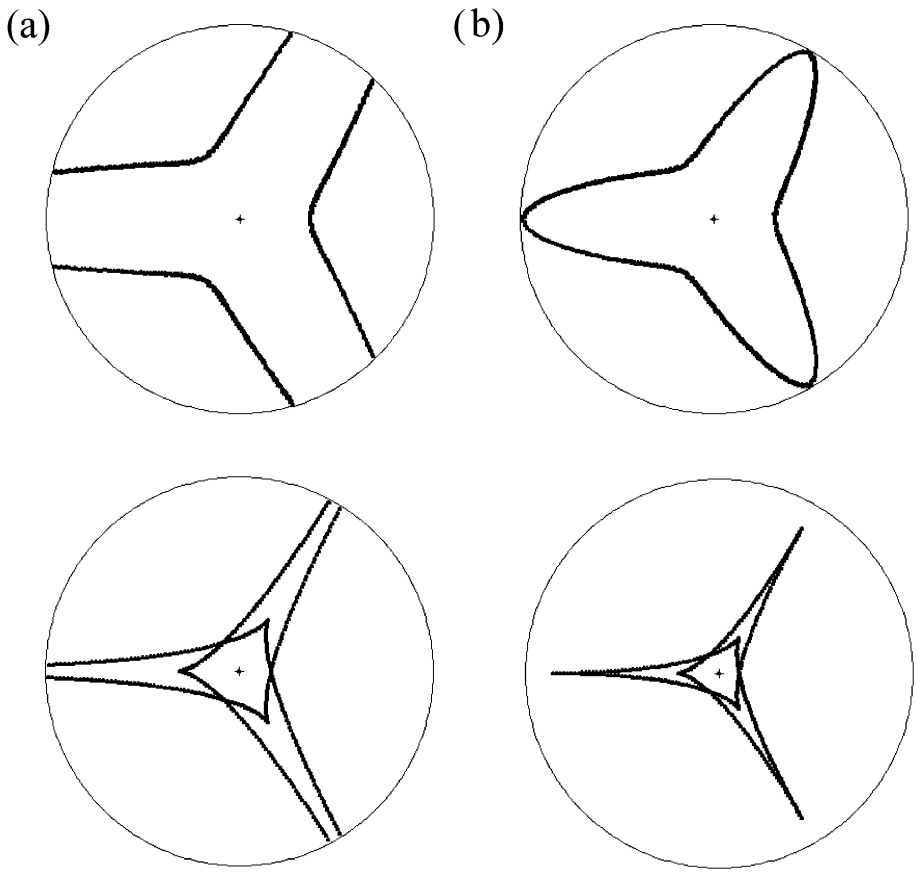

Figure 9. Parabolic lines (upper plots) and caustics (lower plots) for the $S2$ wave near the conical singularity in cubic anisotropy with varying strength. The parameters of anisotropy are: $a_{11} = 6.25$, $a_{44} = 2.08$, (a) $\gamma = 0.75$, (b) $\gamma = 0.60$. The crosses in the upper plots denote the conical singularity that coincides with the vertical axis. The bounding circles correspond to the deviation $\theta = 8^\circ$ of the slowness directions (upper plots) or ray directions (lower plots) from the vertical axis.

Since $\Delta\mathbf{v}^{(23)}$ defined in eq. (41) and ΔG defined in eq. (65) are first-order quantities in ϑ, we obtain

$$H_{il}^{(23)} \ll 1. \tag{69}$$

This implies that $H_{il}^{(23)}$ produces no anomalies in the shape of the slowness sheet in the vicinity of the intersection singularity. Consequently, no parabolic lines can appear in the vicinity of this singularity in weakly anisotropic solids.

6 EXAMPLES

In this section, we demonstrate numerically the results obtained in the previous section. We illustrate the form of parabolic lines and caustics on several examples of anisotropy displaying various symmetries and strengths. We concentrate on the vicinity of singularities, where parabolic lines and caustics are most complicated.

6.1 Kiss singularity

Figs 7 and 8 show the parabolic lines and caustics near a kiss singularity in cubic anisotropy. The kiss singularity is along the vertical axis. The parameters of cubic anisotropy satisfy the following relations: $a_{11} = a_{22} = a_{33}$, $a_{44} = a_{55} = a_{66}$ and $a_{12} = a_{13} = a_{23}$. The remaining parameters are zero. The strength of anisotropy is defined by the parameter $\gamma = a_{12} - a_{11} + 2a_{44}$. We study anisotropy with two different strengths: model (a) shows a very strong anisotropy with anisotropy parameters $a_{11} = 6.25$, $a_{44} = 2.08$ and $\gamma = 2.50$, and model (b) shows a strong anisotropy with anisotropy parameters $a_{11} = 6.25$, $a_{44} = 2.08$ and $\gamma = 1.38$. Fig. 7 shows parabolic lines (upper plots) and caustics (lower plots) for the $S2$ wave, Fig. 8 shows the same for the $S1$ wave.

Model (a) illustrates the case, where the $S2$-wave parabolic lines run around the singularity but do not touch it (see Fig. 7). On the other hand, the $S1$-wave parabolic lines cross the singularity (see Fig. 8). This implies that the parabolic lines on the $S1$ and $S2$ slowness sheets behave independently and that the parabolic lines on the $S1$ slowness sheet only touch the singularity, but do not pass through it. If the lines pass through the singularity, they should jump from one slowness sheet to the other, which is not the case.

Model (b) illustrates the case where parabolic lines touch the singularity simultaneously on both slowness sheets. It also shows that parabolic lines and caustics are significantly more complicated for the $S2$ wave than for the $S1$ wave.

As mentioned, the strength of anisotropy for model (b) is lower than that for model (a). When the anisotropy decreases further, the saddle-shaped area on the $S1$-wave slowness sheet also decreases. For $\gamma = 1.33$, the $S1$-wave parabolic lines disappear near the singularity. They even disappear on the whole $S1$ slowness sheet. For $\gamma = 1.17$, the parabolic lines also disappear near the singularity on the $S2$-wave slowness sheet. Nevertheless, $S2$-wave parabolic lines and caustics still occur in the area near the conical singularity (see the next example).

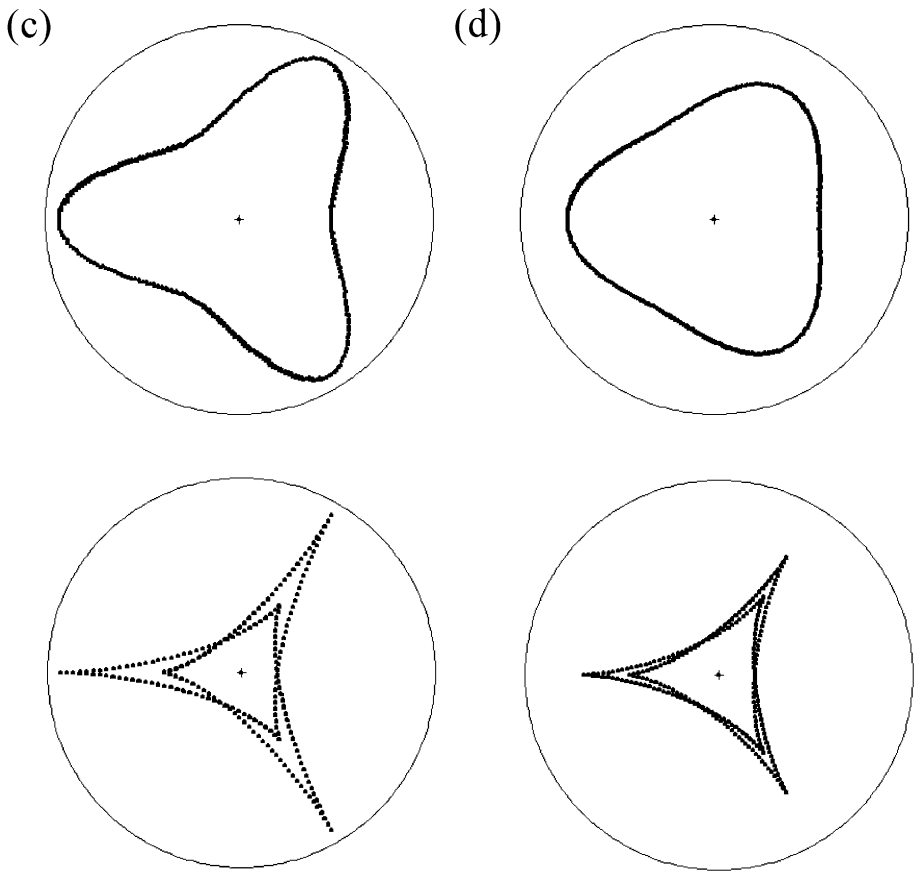

Figure 10. Parabolic lines (upper plots) and caustics (lower plots) for the $S2$ wave near the conical singularity in cubic anisotropy with varying strength. The parameters of anisotropy are: $a_{11} = 6.25$, $a_{44} = 2.08$, (c) $\gamma = 0.40$, (d) $\gamma = 0.20$. The crosses in the upper plots denote the conical singularity that coincides with the vertical axis. The upper bounding circles correspond to the deviation (c) $\theta = 4^\circ$, (d) $\theta = 2^\circ$ of the slowness directions from the vertical axis. The lower bounding circles correspond to the deviation (c) $\theta = 2^\circ$, (d) $\theta = 0.5^\circ$ of ray directions from the vertical axis.

6.2 Conical singularity

Figs 9 and 10 show parabolic lines and caustics near a conical singularity under cubic anisotropy with four different anisotropy strengths. The parameters of anisotropy are: $a_{11} = 6.25$, $a_{44} = 2.08$, (a) $\gamma = 0.75$, (b) $\gamma = 0.60$, (c) $\gamma = 0.40$ and (d) $\gamma = 0.20$. The anisotropy is rotated so that the conical singularity is along the vertical axis. The figures show the $S2$-wave parabolic lines only, because no parabolic lines appear on the $S1$-wave slowness sheet in these anisotropy models. Three pairs of parabolic lines appear on the $S2$ slowness sheet in the strongest anisotropy model studied (Fig. 9a). For decreasing anisotropy, the pairs of parabolic lines interconnect to form one closed curve around the singularity (Fig. 9b). If the anisotropy is further decreased (Fig. 10), the saddle-shaped area inside the curve decreases and the curve contracts closer and closer to the singularity. However, it never disappears for non-zero anisotropy. The parabolic line only disappears together with the singularity when the anisotropy parameter γ is exactly zero, i.e. when the medium becomes isotropic.

Fig. 11 shows two examples of anisotropy with parabolic lines crossing the conical singularity. Conditions for the occurrence of this rather anomalous effect were studied by Shuvalov & Every (1997). The anisotropy studied has a general triclinic symmetry. The conical singularity is along the vertical axis and arises from the kiss singularity in the cubic anisotropy by a small perturbation of the parameters of cubic symmetry. The parameters of the anisotropy are: $a_{11} = a_{22} = a_{33} = 6.25, a_{44} = a_{55} = a_{66} = 2.08, a_{12} = a_{13} = a_{23} = a_{11} - 2a_{44} + \gamma, a_{14} = a_{15} = a_{56} = -a_{24} = -a_{25} = -a_{46} = \varepsilon\, a_{11}$, with values $\varepsilon = 0.02$ and $\gamma = 3.75$ for model (a), and $\varepsilon = 0.007$ and $\gamma = 1.31$ for model (b). The strength of anisotropy for model (b) is approximately three times lower than that for model (a). In both models, parabolic lines cross the singularity on the $S1$ (lower plots) and the $S2$ (upper plots) slowness sheets. The figure shows that the lines pass through the singularity and jump from one slowness sheet to the other. Fig. 12 shows the caustics and anticaustics generated by the conical singularity. Since the parabolic lines pass through the singularity, the caustics of the $S1$ and $S2$ waves form branches of a single closed curve. The caustics of the $S1$ and $S2$ waves are linked at six points, because six parabolic lines pass through the singularity. Moreover, the caustic touches the anticaustic at these six points. As the anisotropy decreases, the parabolic lines passing through the singularity disappear and the caustic around the singularity no longer touches the anticaustic.

6.3 Wedge singularity

Fig. 13 shows the parabolic lines and caustics of the $S2$ wave near a wedge singularity in two anisotropic models. The models arise from a small perturbation of cubic anisotropy. The cubic anisotropy was perturbed by adding a small but non-zero parameter a_{14}. The wedge singularity is along the vertical axis and arose from the kiss singularity in the cubic anisotropy. The resultant anisotropy is monoclinic (see Helbig 1994 eq. 11.48). The parameters of anisotropy are: $a_{11} = a_{22} = a_{33} = 6.25$, $a_{44} = a_{55} = a_{66} = 2.08$, $a_{12} = a_{13} = a_{23} = a_{11} - 2a_{44} + \gamma$, $a_{14} = \varepsilon\, a_{11}$, (a) $\gamma = 0.63$, $\varepsilon = 0.01$, (b) $\gamma = 0.31$, $\varepsilon = 0.005$. The remaining elastic parameters are zero.

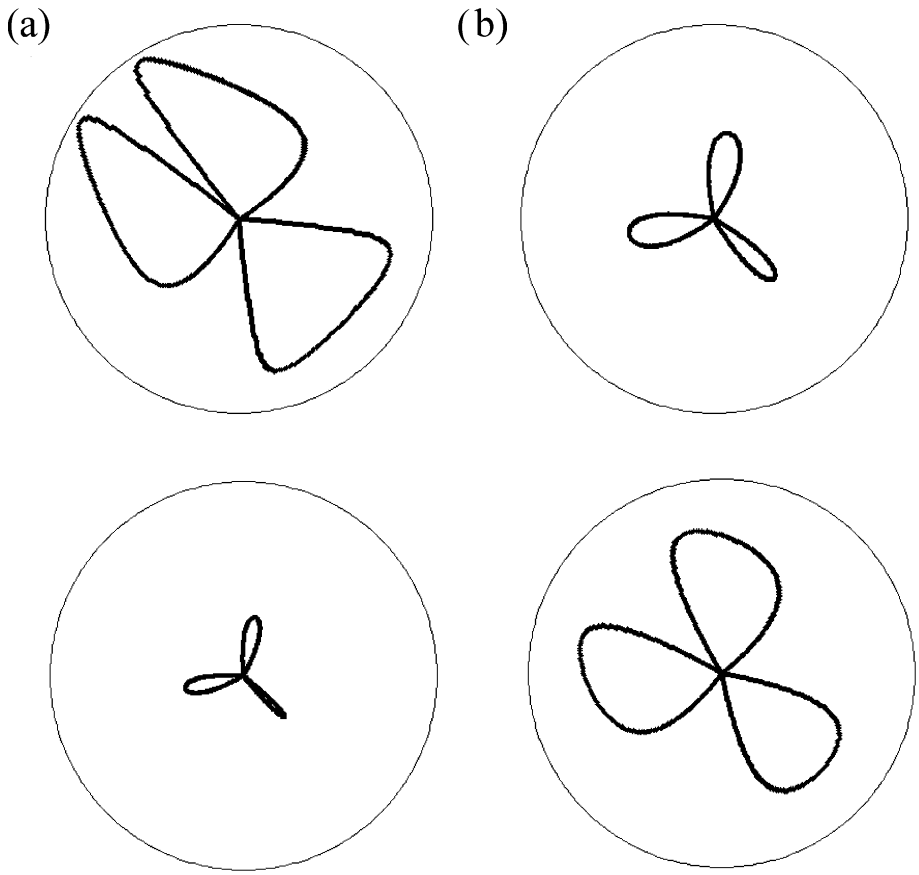

Figure 11. Parabolic lines for the $S2$ (upper plots) and $S1$ (lower plots) waves near a conical singularity for anisotropy models (a) and (b). For parameters of models (a) and (b), see the text. The conical singularity is along the vertical axis. The bounding circles correspond to the deviation $\theta = 2^\circ$ of the slowness directions from the vertical axis.

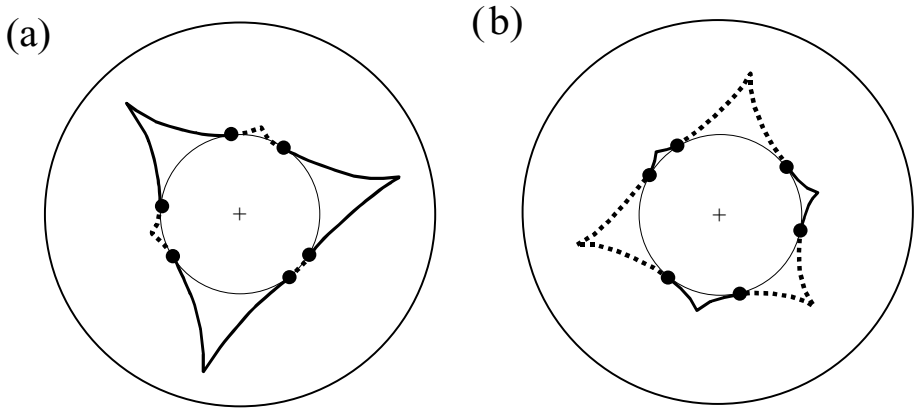

Figure 12. Caustics for the *S*1 (dotted line) and *S*2 (full line) waves near a conical singularity for anisotropy models (a) and (b). For parameters of anisotropy see the text. The conical singularity coincides with the vertical axis. The left/right outer circle corresponds to the deviation $\theta = 12^\circ/4^\circ$ of the ray directions from the vertical axis. The inner circles correspond to the anticaustics generated by the conical singularity. The dots mark points of intersection of the caustic and anticaustic.

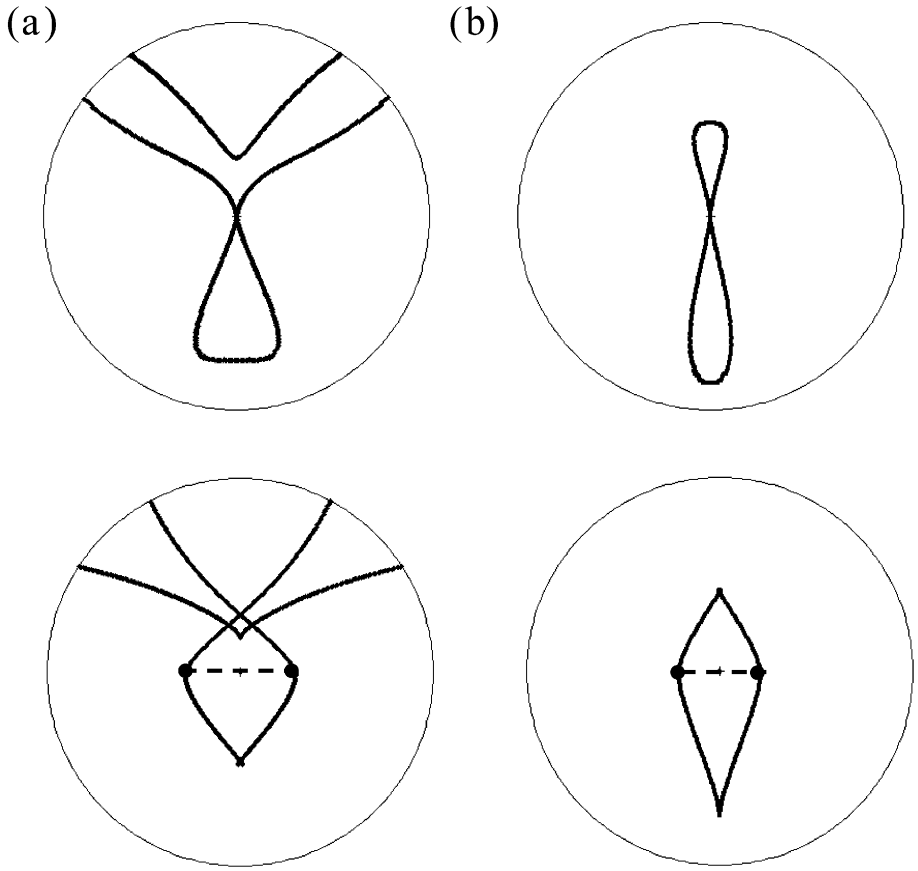

Figure 13. Parabolic lines (upper plots) and caustics (lower plots) for the *S*2 wave near a wedge singularity for anisotropy models (a) and (b). For parameters of anisotropy, see the text. The wedge singularity is along the vertical axis. The bounding circles in the upper plots correspond to the deviation (a) $\theta = 5^\circ$, (b) $\theta = 2.5^\circ$ of the slowness directions from the vertical axis. The bounding circles in the lower plots correspond to the deviation (a) $\theta = 3^\circ$, (b) $\theta = 2^\circ$ of the ray directions from the vertical axis. The dashed line marks the anticaustic. The dots mark points of intersection of the caustic and anticaustic.

The anisotropy in model (b) is twice as weak as that in model (a). In both models, parabolic lines and caustics appear on the *S*2 slowness and wave sheets only. Two pairs of parabolic lines touch the singularity. The singularity generates a linear anticaustic. The anticaustic is perpendicular to the direction of the wedge. The length of the anticaustic depends on the strength of the anisotropy. As the anisotropy decreases by decreasing parameters γ and ε, the length of the anticaustic also decreases. Since parabolic lines touch the singularity, the caustic and anticaustic touch each other. If the anisotropy is decreased, the parabolic lines are concentrated in a close vicinity

of the singularity. For any small but non-zero parameters γ and ε, the parabolic lines always exist and touch the singularity. As the anisotropy decreases, the shape of the parabolic line flattens. Also, the width of the caustic decreases more rapidly than its length. The singularity, parabolic lines, caustic and anticaustic disappear only for strictly zero parameters γ and ε.

7 CONCLUSION

The wave metric tensor defined in eq. (9) can conveniently be used to study the shape of slowness and wave surfaces, and the form of parabolic lines and caustics in homogeneous anisotropic solids. No parabolic lines or caustics can appear for the *P* wave under any symmetry or strength of anisotropy. This includes cases when the *P*-wave slowness sheet touches or intersects the sheets of the other waves. Parabolic lines and caustics can appear for the *S*1 and *S*2 waves and separate convex, saddle-shaped and concave areas on the slowness and wave sheets. In general, the form of parabolic lines and caustics is more complicated for the *S*2 wave than for the *S*1 wave. The parabolic lines and caustics can appear, particularly, in the vicinity of singularities. The conical and wedge singularities also generate anticaustics. The conical singularity generates an elliptical or circular anticaustic, the wedge singularity generates a linear anticaustic. The geometry of parabolic lines and caustics can be very complicated in the vicinity of singularities. The parabolic lines can even touch a singularity: they can touch wedge and kiss singularities or pass through a conical singularity. The parabolic lines can coincide with an intersection singularity. If the parabolic lines pass through a conical singularity, a composite caustic is generated with its branches on the *S*1 and *S*2 wave sheets. This caustic touches the anticaustic at isolated points.

The form of the parabolic lines and caustics simplifies in weakly anisotropic solids. Under sufficiently weak anisotropy, no parabolic lines and caustics appear on the *S*1 slowness or wave sheets. Parabolic lines and caustics can appear for the *S*2 wave, but only in directions close to conical or wedge singularities. Each conical or wedge singularity in weakly anisotropic solids generates parabolic lines, caustics and anticaustics in its vicinity. In contrast with strong anisotropy, the parabolic lines cannot pass through or touch the conical singularity in weak anisotropy. The caustic cannot touch the anticaustic. On the other hand, the parabolic lines touch each wedge singularity, and the caustic must touch the anticaustic associated with this singularity. The size of the caustics and anticaustics decreases with decreasing strength of anisotropy. Under infinitesimally weak anisotropy, the caustics and anticaustics contract into a single common point. For isotropy, the conical and wedge singularities disappear together with the caustics and anticaustics associated with them.

As regards transverse isotropy, we can draw the following conclusion: since weak transverse isotropy forms no conical or wedge singularities, no parabolic lines, caustics or triplications can appear in this symmetry, provided the anisotropy is sufficiently weak.

ACKNOWLEDGMENTS

I thank Vlastislav Červený for stimulating discussions on the subject, and Veronique Farra, Klaus Helbig, Ivan Pšenčík, Michael Slawiński and an anonymous reviewer for their reviews. The work was supported by the Consortium Project 'Seismic waves in complex 3-D structures', and by the Grant Agency of the Czech Republic, Grant No 205/00/1350.

REFERENCES

Aki, K. & Richards, P.G., 1980. *Quantitative Seismology, Theory and Methods*, Freeman, San Francisco.

Babich, V.M., 1961. Ray method of calculating the intensity of wavefronts in the case of a heterogeneous, anisotropic, elastic medium (in Russian), in *Problems of the Dynamic Theory of Propagation of Seismic Waves*, Vol. V, pp. 36–46, Leningrad University Press, republished in 1994, *Geophys. J. Int.,* **118,** 379–383.

Bakker, P.M., 1998. Phase shift at caustics along rays in anisotropic media, *Geophys. J. Int.,* **134,** 515–518.

Boulanger, Ph. & Hayes, M., 1998. Acoustic axes for elastic waves in crystals: theory and applications, *Proc. R. Soc. Lond.,* A., **454,** 2323–2346.

Burridge, R., 1967. The singularity on the plane lids of the wave surface of elastic media with cubic symmetry, *Q. J. Mech. Appl. Math.,* **20,** 40–56.

Červený, V., 2001. *Seismic Ray Theory,* Cambridge University Press, Cambridge.

Červený, V., 2002. Fermat's variational principle for anisotropic inhomogeneous media, *Stud. Geophys. Geod.,* **46,** 567–588.

Crampin, S. & Yedlin, M., 1981. Shear-wave singularities of wave propagation in anisotropic media, *J. Geophys.,* **49,** 43–46.

Every, A.G. & Kim, K.Y., 1994. Time domain dynamic response functions of elastically anisotropic solids, *J. acoust. Soc. Am.,* **95,** 2505–2516.

Farra, V., 2001. High-order perturbations of the phase velocity and polarization of *qP* and *qS* waves in anisotropic media, *Geophys. J. Int.,* **147,** 93–104.

Gajewski, D. & Pšenčík, I., 1990. Vertical seismic profile synthetics by dynamic ray tracing in laterally varying layered anisotropic structures, *J. geophys. Res.,* **95,** 11 301–11 315.

Grechka, V.Yu. & Obolentseva, I.R., 1993. Geometrical structure of shear wave surfaces near singularity directions in anisotropic media, *Geophys. J. Int.,* **115,** 609–616.

Hanyga, A., ed., 1984. *Seismic Wave Propagation in the Earth,* Elsevier, Amsterdam.

Helbig, K., 1994. *Foundations of Anisotropy for Exploration Seismics,* Pergamon, New York.

Jech, J. & Pšenčík, I., 1989. First-order perturbation method for anisotropic media, *Geophys. J. Int.,* **99,** 369–376.

Klimeš, L., 2002. Relation of the wave-propagation metric tensor to the curvatures of the slowness and ray-velocity surfaces, *Stud. Geophys. Geod.,* **46,** 589–597.

Kravtsov, Yu.A. & Orlov, Yu.I., 1990. *Geometrical Optics of Inhomogeneous Media,* Springer-Verlag, New York.

Musgrave, M.J.P., 1970. *Crystal Acoustics,* Holden-Day, London.

Musgrave, M.J.P., 1985. Acoustic axes in orthorhombic media, *Proc. R. Soc. Lond.,* A., **401,** 131–143.

Payton, R.G., 1992. Wave propagation in a restricted transversely isotropic elastic solid whose slowness surface contains conical points, *Q. J. Mech. Appl. Math.,* **45,** 183–197.

Pšenčík, I., 1998. Green's functions for inhomogeneous weakly anisotropic media, *Geophys. J. Int.,* **135,** 279–288.

Rümpker, G. & Thomson, C.J., 1994. Seismic-waveform effects of conical points in gradually varying anisotropic media, *Geophys. J. Int.,* **118,** 759–780.

Shuvalov, A.L., 1998. Topological features of the polarization fields of plane acoustic waves in anisotropic media, *Proc. R. Soc. Lond.,* A., **454,** 2911–2947.

Shuvalov, A.L. & Every, A.G., 1996. Curvature of acoustic slowness surface of anisotropic solids near symmetry axes, *Phys. Rev.,* B., **53,** 14 906–14 916.

Shuvalov, A.L. & Every, A.G., 1997. Shape of the acoustic slowness surface of anisotropic solids near points of conical degeneracy, *J. acoust. Soc. Am.,* **101,** 2381–2382.

Thomsen, L., 1986. Weak elastic anisotropy, *Geophysics,* **51,** 1954–1966.

Vavryčuk, V., 2001. Ray tracing in anisotropic media with singularities, *Geophys. J. Int.,* **145,** 265–276.

Vavryčuk, V., 2002. Asymptotic elastodynamic Green function in the kiss singularity in homogeneous anisotropic solids, *Stud. Geophys. Geod.,* **46,** 249–266.

Vavryčuk, V. & Yomogida, K., 1996. *SH*-wave Green tensor for homogeneous transversely isotropic media by higher-order approximations in asymptotic ray theory, *Wave Motion,* **23,** 83–93.

Wolfe, J.P., 1998. *Imaging Phonons. Acoustic Wave Propagation in Solids,* Cambridge University Press, Cambridge.

APPENDIX A: PERTURBATION THEORY FOR A DEGENERATE CHRISTOFFEL EIGENVALUE PROBLEM

Assume that the Christoffel tensor Γ_{jk} is nearly degenerate

$$\Gamma_{jk} = \Gamma^0_{jk} + \Delta\Gamma_{jk}, \tag{A1}$$

where $\Delta\,\Gamma_{jk}$ is a small perturbation from the degenerate tensor Γ^0_{jk} with eigenvalues

$$G^{0(1)} \neq G^{0(2)} = G^{0(3)} \equiv G^{0(23)}. \tag{A2}$$

The eigenvector of Γ^0_{jk} corresponding to the non-degenerate eigenvalue $G^{0(1)}$ is $\widehat{\mathbf{g}}^{0(1)}$, the eigenvectors corresponding to the degenerate eigenvalues $G^{0(2)}$ and $G^{0(3)}$ are $\widehat{\mathbf{g}}^{0(2)}$ and $\widehat{\mathbf{g}}^{0(3)}$. Vectors $\widehat{\mathbf{g}}^{0(2)}$ and $\widehat{\mathbf{g}}^{0(3)}$ form an arbitrary frame of orthogonal vectors perpendicular to $\widehat{\mathbf{g}}^{0(1)}$. Using perturbation theory (see Shuvalov 1998; Farra 2001), the approximate formulae for eigenvalues $G^{(2)}$ and $G^{(3)}$ of Γ_{jk} can be expressed as follows:

$$G^{(2),(3)} = \frac{1}{2}\left[\widehat{M}^{(22)} + \widehat{M}^{(33)} \pm \Delta G\right]. \tag{A3}$$

$$\Delta G = G^{(2)} - G^{(3)} = \sqrt{\left[\widehat{M}^{(22)} - \widehat{M}^{(33)}\right]^2 + 4\left[\widehat{M}^{(23)}\right]^2}, \tag{A4}$$

where

$$\widehat{M}^{(KL)} = \widehat{m}^{(KL)} + \frac{\widehat{m}^{(1K)}\widehat{m}^{(1L)}}{G^{0(23)} - G^{0(1)}}, \quad K, L = 2, 3, \tag{A5}$$

$$\widehat{m}^{(rs)} = \Gamma_{jk}\widehat{g}^{0(r)}_j\widehat{g}^{0(s)}_k, \quad r, s = 1, 2, 3. \tag{A6}$$

Let us introduce base vectors $\mathbf{g}^{0(1)} = \widehat{\mathbf{g}}^{0(1)}$, $\mathbf{g}^{0(2)}$ and $\mathbf{g}^{0(3)}$,

$$\mathbf{g}^{0(2)} = \widehat{\mathbf{g}}^{0(2)}\cos\Phi + \widehat{\mathbf{g}}^{0(3)}\sin\Phi, \tag{A7}$$

$$\mathbf{g}^{0(3)} = -\widehat{\mathbf{g}}^{0(2)}\sin\Phi + \widehat{\mathbf{g}}^{0(3)}\cos\Phi. \tag{A8}$$

The angle Φ satisfies the equation

$$\tan 2\Phi = \frac{2\,\widehat{M}^{(23)}}{\widehat{M}^{(22)} - \widehat{M}^{(33)}}, \tag{A9}$$

and is determined as

$$\Phi = \frac{1}{2}\operatorname{atan}\frac{2\,\widehat{M}^{(23)}}{\widehat{M}^{(22)} - \widehat{M}^{(33)}}, \quad \text{for} \quad \widehat{M}^{(22)} - \widehat{M}^{(33)} > 0, \tag{A10}$$

$$\Phi = \frac{\pi}{2} + \frac{1}{2}\operatorname{atan}\frac{2\,\widehat{M}^{(23)}}{\widehat{M}^{(22)} - \widehat{M}^{(33)}}, \quad \text{for} \quad \widehat{M}^{(22)} - \widehat{M}^{(33)} < 0. \tag{A11}$$

Approximate eigenvectors $\mathbf{g}^{(2)}$ and $\mathbf{g}^{(3)}$ of Γ_{jk} are then expressed as follows:

$$\mathbf{g}^{(2)} = \mathbf{g}^{0(2)} + \mathbf{g}^{0(1)}\frac{m^{(12)}}{G^{0(23)} - G^{0(1)}}, \tag{A12}$$

$$\mathbf{g}^{(3)} = \mathbf{g}^{0(3)} + \mathbf{g}^{0(1)}\frac{m^{(13)}}{G^{0(23)} - G^{0(1)}}. \tag{A13}$$

The matrix $m^{(rs)}$ is calculated from eq. (A6) using the base vectors $\mathbf{g}^{0(r)}$, $r = 1, 2, 3$. Note that vectors $\mathbf{g}^{0(2)}$ and $\mathbf{g}^{0(3)}$ are perpendicular to $\mathbf{g}^{0(1)} = \widehat{\mathbf{g}}^{0(1)}$ in the same fashion as vectors $\widehat{\mathbf{g}}^{0(2)}$ and $\widehat{\mathbf{g}}^{0(3)}$, hence they can serve as eigenvectors of Γ^0_{jk}. However, these eigenvectors are exceptional, because in perturbing from the degenerate tensor Γ^0_{jk} to the non-degenerate tensor Γ_{jk} the transition from eigenvectors $\mathbf{g}^{0(2)}$ and $\mathbf{g}^{0(3)}$ to eigenvectors $\mathbf{g}^{(2)}$ and $\mathbf{g}^{(3)}$ is continuous. No other eigenvectors display this property. Furthermore, some formulae simplify when these exceptional base vectors are used. For example,

$$M^{(23)} = 0, \tag{A14}$$

$$\Delta G = M^{(22)} - M^{(33)}, \tag{A15}$$

$$\Phi = 0. \tag{A16}$$

The matrix $M^{(KL)}$ is calculated from eq. (A5) using the base vectors $\mathbf{g}^{0(r)}$, $r = 1, 2, 3$.

The formulae for eigenvectors/eigenvalues are valid up to the first/second order of perturbation, respectively.

APPENDIX B: EIGENVALUES AND EIGENVECTORS OF Γ_{jk} IN WEAK ANISOTROPY FOR A FIXED SLOWNESS DIRECTION

Let us assume that the medium is weakly anisotropic

$$a_{ijkl} = a^0_{ijkl} + \Delta a_{ijkl}, \tag{B1}$$

$$a^0_{ijkl} = (\alpha^2 - 2\beta^2)\delta_{ij}\delta_{kl} + \beta^2(\delta_{ik}\delta_{jl} + \delta_{il}\delta_{jk}), \tag{B2}$$

where α and β are the *P*- and *S*-wave velocities in the isotropic reference medium, δ_{ij} is the Kronecker delta, and Δa_{ijkl} are small perturbations from the parameters of the isotropic reference medium a^0_{ijkl}. Perturbing the Christoffel tensor by perturbing the elastic parameters of the medium, we obtain

$$\Gamma^0_{jk} = (\alpha^2 - \beta^2)n_j n_k + \beta^2\delta_{jk}, \tag{B3}$$

$$\Delta\Gamma_{jk} = \Delta a_{ijkl}n_i n_l, \tag{B4}$$

where Γ^0_{jk} is the Christoffel tensor in the isotropic reference medium and $\Delta\Gamma_{jk}$ is its perturbation. If we introduce the weak anisotropy tensor b_{ijkl}

$$\Delta a_{ijkl} = \varepsilon b_{ijkl}, \tag{B5}$$

where ε is a small and positive parameter, we can express ΔG defined in eq. (A4) as follows:

$$\Delta G = G^{(2)} - G^{(3)} = \varepsilon\sqrt{\left[\widehat{\mathbf{u}}^{b(23)}\cdot\mathbf{n} + \varepsilon\mathbf{n}^{\mathrm{T}}\widehat{\mathbf{F}}\mathbf{n}\right]^2 + \left[\widehat{\mathbf{v}}^{b(23)}\cdot\mathbf{n} + \varepsilon\mathbf{n}^{\mathrm{T}}\widehat{\mathbf{G}}\mathbf{n}\right]^2}, \tag{B6}$$

where

$$\widehat{u}^{b(rs)}_i = b_{ijkl}n_l\left[\widehat{g}^{0(r)}_j\widehat{g}^{0(r)}_k - \widehat{g}^{0(s)}_j\widehat{g}^{0(s)}_k\right],$$

$$\widehat{v}_i^{b(rs)} = b_{ijkl} n_l \left[\widehat{g}_j^{0(r)} \widehat{g}_k^{0(s)} + \widehat{g}_j^{0(s)} \widehat{g}_k^{0(r)} \right], \tag{B7}$$

$$\widehat{F}_{il} = \frac{1}{4} \frac{\widehat{v}_i^{b(12)} \widehat{v}_l^{b(12)} - \widehat{v}_i^{b(13)} \widehat{v}_l^{b(13)}}{\beta^2 - \alpha^2},$$

$$\widehat{G}_{il} = \frac{1}{4} \frac{\widehat{v}_i^{b(12)} \widehat{v}_l^{b(13)} + \widehat{v}_i^{b(13)} \widehat{v}_l^{b(12)}}{\beta^2 - \alpha^2}. \tag{B8}$$

Vectors $\mathbf{g}^{0(2)}$ and $\mathbf{g}^{0(3)}$ are defined in eqs (A7) and (A8) with angle Φ

$$\tan 2\Phi = \frac{\widehat{\mathbf{v}}^{b(23)} \cdot \mathbf{n} + \varepsilon \mathbf{n}^{\mathrm{T}} \widehat{\mathbf{G}} \mathbf{n}}{\widehat{\mathbf{u}}^{b(23)} \cdot \mathbf{n} + \varepsilon \mathbf{n}^{\mathrm{T}} \widehat{\mathbf{F}} \mathbf{n}}. \tag{B9}$$

Expressing $m^{(1,J)}$, $J = 2, 3$ required in eqs (A12) and (A13) as

$$m^{(1,J)} = \frac{1}{2} \varepsilon \mathbf{v}^{b(1,J)} \cdot \mathbf{n}, \tag{B10}$$

we arrive at the approximate formulae for eigenvectors $\mathbf{g}^{(2)}$ and $\mathbf{g}^{(3)}$,

$$\mathbf{g}^{(2)} = \mathbf{g}^{0(2)} + \Delta \mathbf{g}^{(2)} = \mathbf{g}^{0(2)} + \frac{1}{2} \varepsilon \mathbf{g}^{0(1)} \frac{\mathbf{v}^{b(12)} \cdot \mathbf{n}}{\beta^2 - \alpha^2}, \tag{B11}$$

$$\mathbf{g}^{(3)} = \mathbf{g}^{0(3)} + \Delta \mathbf{g}^{(3)} = \mathbf{g}^{0(3)} + \frac{1}{2} \varepsilon \mathbf{g}^{0(1)} \frac{\mathbf{v}^{b(13)} \cdot \mathbf{n}}{\beta^2 - \alpha^2}, \tag{B12}$$

where $\mathbf{g}^{0(1)}$ equals $\mathbf{n}$, and vectors $\mathbf{v}^{b(12)}$ and $\mathbf{v}^{b(13)}$ are calculated from eq. (B7) using base vectors $\mathbf{g}^{0(r)}$, $r = 1, 2, 3$.

If we substitute the base vectors $\widehat{\mathbf{g}}^{0(r)}$ by $\mathbf{g}^{0(r)}$ in eqs (B6) and (B9) we obtain

$$\Delta G = \varepsilon [\mathbf{u}^{b(23)} \cdot \mathbf{n} + \varepsilon \mathbf{n}^{\mathrm{T}} \mathbf{F} \mathbf{n}], \tag{B13}$$

$$\Phi = 0, \tag{B14}$$

where $\mathbf{u}^{b(23)}$ and $\mathbf{F}$ are calculated from eqs (B7) and (B8) using the base vectors $\mathbf{g}^{0(r)}$.

The formulae for eigenvectors/eigenvalues are valid up to the first/second order of perturbation, respectively.

APPENDIX C: EIGENVALUES AND EIGENVECTORS OF Γ_{jk} IN THE VICINITY OF A SINGULARITY IN A MEDIUM WITH FIXED ELASTIC PARAMETERS

All quantities at the singularity are denoted by superscript 0. The slowness direction is perturbed as follows (see Fig. 6):

$$\mathbf{n} = \mathbf{n}^0 + \Delta \mathbf{n}, \quad \Delta \mathbf{n} = \vartheta \mathbf{e} - \frac{1}{2} \vartheta^2 \mathbf{n}^0, \tag{C1}$$

where $\mathbf{e}$ is an arbitrary unit vector orthogonal to $\mathbf{n}^0$, and ϑ is a small angle between $\mathbf{n}$ and $\mathbf{n}^0$. Perturbing the Christoffel tensor by perturbing the slowness direction $\mathbf{n}$ we obtain

$$\Gamma^0_{jk} = a_{ijkl} n_i^0 n_l^0, \tag{C2}$$

$$\Delta \Gamma_{jk} = a_{ijkl} \left(\Delta n_i n_l^0 + \Delta n_l n_i^0 \right) + a_{ijkl} \Delta n_i \Delta n_l. \tag{C3}$$

Inserting eqs (C2) and (C3) into eq. (A4) we derive (see Shuvalov 1998, eqs 2.11–2.17)

$$\Delta G = \vartheta \sqrt{\left[2 \widehat{\mathbf{u}}^{0(23)} \cdot \mathbf{e} + \vartheta \mathbf{e}^{\mathrm{T}} \widehat{\mathbf{F}} \mathbf{e} \right]^2 + \left[2 \widehat{\mathbf{v}}^{0(23)} \cdot \mathbf{e} + \vartheta \mathbf{e}^{\mathrm{T}} \widehat{\mathbf{G}} \mathbf{e} \right]^2}, \tag{C4}$$

where

$$\widehat{u}_i^{0(rs)} = a_{ijkl} n_l^0 \left[\widehat{g}_j^{0(r)} \widehat{g}_k^{0(r)} - \widehat{g}_j^{0(s)} \widehat{g}_k^{0(s)} \right],$$

$$\widehat{v}_i^{0(rs)} = a_{ijkl} n_l^0 \left[\widehat{g}_j^{0(r)} \widehat{g}_k^{0(s)} + \widehat{g}_j^{0(s)} \widehat{g}_k^{0(r)} \right], \tag{C5}$$

$$\widehat{F}_{il} = a_{ijkl} \left[\widehat{g}_j^{0(2)} \widehat{g}_k^{0(2)} - \widehat{g}_j^{0(3)} \widehat{g}_k^{0(3)} \right] + \frac{\widehat{v}_i^{0(12)} \widehat{v}_l^{0(12)} - \widehat{v}_i^{0(13)} \widehat{v}_l^{0(13)}}{G^{0(23)} - G^{0(1)}}, \tag{C6}$$

$$\widehat{G}_{il} = a_{ijkl} \left[\widehat{g}_j^{0(2)} \widehat{g}_k^{0(3)} + \widehat{g}_j^{0(3)} \widehat{g}_k^{0(2)} \right] + \frac{\widehat{v}_i^{0(12)} \widehat{v}_l^{0(13)} + \widehat{v}_i^{0(13)} \widehat{v}_l^{0(12)}}{G^{0(23)} - G^{0(1)}}. \tag{C7}$$

The vectors $\mathbf{g}^{0(2)}$ and $\mathbf{g}^{0(3)}$ are defined in eqs (A7) and (A8) with angle Φ

$$\tan 2\Phi = \frac{2 \widehat{\mathbf{v}}^{0(23)} \cdot \mathbf{e} + \vartheta \mathbf{e}^{\mathrm{T}} \widehat{\mathbf{G}} \mathbf{e}}{2 \widehat{\mathbf{u}}^{0(23)} \cdot \mathbf{e} + \vartheta \mathbf{e}^{\mathrm{T}} \widehat{\mathbf{F}} \mathbf{e}}. \tag{C8}$$

Expressing $m^{(1,J)}$, $J = 2, 3$ required in eqs (A12) and (A13) as

$$m^{(1,J)} = \vartheta \mathbf{v}^{0(1,J)} \cdot \mathbf{e}, \tag{C9}$$

we arrive at the approximate formulae for eigenvectors $\mathbf{g}^{(2)}$ and $\mathbf{g}^{(3)}$,

$$\mathbf{g}^{(2)} = \mathbf{g}^{0(2)} + \Delta \mathbf{g}^{(2)} = \mathbf{g}^{0(2)} + \vartheta \mathbf{g}^{0(1)} \frac{\mathbf{v}^{0(12)} \cdot \mathbf{e}}{G^{0(23)} - G^{0(1)}}, \tag{C10}$$

$$\mathbf{g}^{(3)} = \mathbf{g}^{0(3)} + \Delta \mathbf{g}^{(3)} = \mathbf{g}^{0(3)} + \vartheta \mathbf{g}^{0(1)} \frac{\mathbf{v}^{0(13)} \cdot \mathbf{e}}{G^{0(23)} - G^{0(1)}}, \tag{C11}$$

where vectors $\mathbf{v}^{0(12)}$ and $\mathbf{v}^{0(13)}$ are calculated from eq. (C5) using base vectors $\mathbf{g}^{0(r)}$, $r = 1, 2, 3$.

If we substitute base vectors $\widehat{\mathbf{g}}^{0(r)}$ by $\mathbf{g}^{0(r)}$ in eqs (C4) and (C8) we obtain

$$\Delta G = \vartheta \left[2 \mathbf{u}^{0(23)} \cdot \mathbf{e} + \vartheta \mathbf{e}^{\mathrm{T}} \mathbf{F} \mathbf{e} \right], \tag{C12}$$

$$\Phi = 0, \tag{C13}$$

where $\mathbf{u}^{0(23)}$ and $\mathbf{F}$ are calculated from eqs (C5) and (C6) using base vectors $\mathbf{g}^{0(r)}$.

The formulae for eigenvectors/eigenvalues are valid up to the first/second order of perturbation, respectively.

APPENDIX D: THE WAVE METRIC TENSOR IN WEAKLY ANISOTROPIC SOLIDS

All quantities expressed in the isotropic reference medium are denoted by a superscript 0. The $S1$-wave metric tensor $H^{(2)}_{il}$ for weakly anisotropic solids is perturbed as follows:

$$H^{(2)}_{il} = H^{0(2)}_{il} + \Delta H^{(2)}_{il}, \tag{D1}$$

where $H^{0(2)}_{il}$ is the leading term of the metric tensor and $\Delta H^{(2)}_{il}$ is its perturbation. Taking into account eq. (18) we obtain

$$H^{0(2)}_{il} = \left[a_{ijkl} g_j^{(2)} g_k^{(2)} \right]^0 + \left[\frac{v_i^{(12)} v_l^{(12)}}{G^{(2)} - G^{(1)}} \right]^0 + \left[\frac{v_i^{(23)} v_l^{(23)}}{G^{(2)} - G^{(3)}} \right]^0, \tag{D2}$$

$$\Delta H_{il}^{(2)} = \Delta\left[a_{ijkl} g_j^{(2)} g_k^{(2)}\right] + \Delta\left[\frac{v_i^{(12)} v_l^{(12)}}{G^{(2)} - G^{(1)}}\right] + \Delta\left[\frac{v_i^{(23)} v_l^{(23)}}{G^{(2)} - G^{(3)}}\right]. \tag{D3}$$

The leading terms in eq. (D2) can further be simplified using the following identities:

$$\left[a_{ijkl} g_j^{(2)} g_k^{(2)}\right]^0 = a_{ijkl}^0 g_j^{0(2)} g_k^{0(2)} = (\alpha^2 - \beta^2) g_i^{0(2)} g_l^{0(2)} + \beta^2 \delta_{il}, \tag{D4}$$

$$\left[\frac{v_i^{(12)} v_l^{(12)}}{G^{(2)} - G^{(1)}}\right]^0 = \frac{v_i^{0(12)} v_l^{0(12)}}{G^{0(2)} - G^{0(1)}} = -(\alpha^2 - \beta^2) g_i^{0(2)} g_l^{0(2)}, \tag{D5}$$

$$\left[\frac{v_i^{(23)} v_l^{(23)}}{G^{(2)} - G^{(3)}}\right]^0 = \frac{v_i^{0(23)} v_l^{0(23)} + \Delta v_i^{(23)} v_l^{0(23)} + v_i^{0(23)} \Delta v_l^{(23)}}{\Delta G} = 0, \tag{D6}$$

where we have used

$$a_{ijkl}^0 = (\alpha^2 - 2\beta^2)\delta_{ij}\delta_{kl} + \beta^2(\delta_{ik}\delta_{jl} + \delta_{il}\delta_{jk}), \tag{D7}$$

$$G^{0(1)} = \alpha^2, \quad G^{0(2)} = G^{0(3)} = \beta^2, \tag{D8}$$

$$v_i^{0(12)} = a_{ijkl}^0 n_l \left[g_j^{0(1)} g_k^{0(2)} + g_j^{0(2)} g_k^{0(1)}\right] = (\alpha^2 - \beta^2) g_i^{0(2)}, \tag{D9}$$

$$v_i^{0(23)} = a_{ijkl}^0 n_l \left[g_j^{0(2)} g_k^{0(3)} + g_j^{0(3)} g_k^{0(2)}\right] = 0. \tag{D10}$$

The quantity $\Delta G = G^{(2)} - G^{(3)}$ is small and positive. Using eqs (D4)–(D6), we obtain for the leading term $H_{il}^{0(2)}$,

$$H_{il}^{0(2)} = \beta^2 \delta_{il}. \tag{D11}$$

The first-order perturbation terms in eq. (D3) have the form

$$\Delta\left[a_{ijkl} g_j^{(2)} g_k^{(2)}\right] = \Delta a_{ijkl} g_j^{0(2)} g_k^{0(2)} + a_{ijkl}^0\left[\Delta g_j^{(2)} g_k^{0(2)} + g_j^{0(2)} \Delta g_k^{(2)}\right], \tag{D12}$$

$$\Delta\left[\frac{v_i^{(12)} v_l^{(12)}}{G^{(2)} - G^{(1)}}\right] = \frac{\Delta v_i^{(12)} v_l^{0(12)} + v_i^{0(12)} \Delta v_l^{(12)}}{G^{0(2)} - G^{0(1)}} - v_i^{0(12)} v_l^{0(12)} \frac{\Delta G^{(2)} - \Delta G^{(1)}}{\left[G^{0(2)} - G^{0(1)}\right]^2}, \tag{D13}$$

$$\Delta\left[\frac{v_i^{(23)} v_l^{(23)}}{\Delta G}\right] = \frac{\Delta v_i^{(23)} \Delta v_l^{(23)}}{\Delta G}, \tag{D14}$$

where ΔG is defined in eq. (B6). Inserting eqs (D7)–(D9) into eqs (D12)–(D14), we obtain for $\Delta H_{il}^{(2)}$,

$$\Delta H_{il}^{(2)} = \Delta a_{ijkl} g_j^{0(2)} g_k^{0(2)} + \left(\alpha^2 - \beta^2\right)\left[\Delta g_i^{(2)} g_l^{0(2)} + g_i^{0(2)} \Delta g_l^{(2)}\right] - g_i^{0(2)} \Delta v_l^{(12)} - g_l^{0(2)} \Delta v_i^{(12)} - g_i^{0(2)} g_l^{0(2)} [\Delta G^{(2)} - \Delta G^{(1)}] + \frac{\Delta v_i^{(23)} \Delta v_l^{(23)}}{\Delta G}, \tag{D15}$$

where

$$\Delta v_i^{(rs)} = \Delta a_{ijkl} n_l \left[g_j^{0(r)} g_k^{0(s)} + g_j^{0(s)} g_k^{0(r)}\right] + a_{ijkl}^0 n_l \left[\Delta g_j^{(r)} g_k^{0(s)} + g_j^{0(r)} \Delta g_k^{(s)} + \Delta g_j^{(s)} g_k^{0(r)} + g_j^{0(s)} \Delta g_k^{(r)}\right]. \tag{D16}$$

By analogy, we obtain the formulae for the metric tensor of the $S2$ wave:

$$H_{il}^{0(3)} = \beta^2 \delta_{il}, \tag{D17}$$

$$\Delta H_{il}^{(3)} = \Delta a_{ijkl} g_j^{0(3)} g_k^{0(3)} + (\alpha^2 - \beta^2)\left[\Delta g_i^{(3)} g_l^{0(3)} + g_i^{0(3)} \Delta g_l^{(3)}\right] - g_i^{0(3)} \Delta v_l^{(13)} - g_l^{0(3)} \Delta v_i^{(13)} - g_i^{0(3)} g_l^{0(3)} [\Delta G^{(3)} - \Delta G^{(1)}] - \frac{\Delta v_i^{(23)} \Delta v_l^{(23)}}{\Delta G}. \tag{D18}$$